IEEE Access
Multidisciplinary | Rapid Review | Open Access Journal

Date of publication xxxx 00, 0000, date of current version xxxx 00, 0000.

Digital Object Identifier 10.1109/ACCESS.2017.DOI

Performance Enhancement of V2V Communication by QC-LDPC Code and NOMA-UM-MIMO Techniques

MARYAM MOHAMMED F. ABDULLAH[1], OSAMA ALLUHAIBI[2],ASIM EGEMEN YILMAZ[3], AYKUT KALAYCIOGLU[4]

[1]Electrical Engineering Department, Ankara, Turkey (e-mail: mfnabdullah@ankara.edu.tr)
[2]Electrical Engineering Department, Kirkuk, IRAQ (e-mail:osake@uokirkuk.edu.iq)
[3]Electrical Engineering Department, Ankara, Turkey (e-mail:aeyilmaz@eng.ankara.edu.tr)
[4]Electrical Engineering Department, Ankara, Turkey (e-mail:kalaycioglu@ankara.edu.tr)

Corresponding author: Maryam Mohammed F. Abdullah (e-mail: mfnabdullah@ankara.edu.tr).

ABSTRACT This study addresses the critical challenges in Vehicle-to-Vehicle (V2V) communications, particularly the issues of high mobility, dynamic channel conditions, and interference that adversely affect Bit Error Rate (BER) performance and overall system capacity. We propose an innovative integration of NOMA with a specific form of Quasi Cyclic-Low Density Parity Check (QC-LDPC) coding to enhance communication reliability and efficiency in vehicular environments, ensuring effective system operation even without clustering. Analytical and numerical simulations based on the NOMA-MIMO system are conducted to derive BER formulas for both near (Bob_1) and far (Bob_2) users. The effectiveness of Successive Interference Cancellation (SIC) techniques in mitigating interference in vehicular environments is also explored. Additionally, mathematical formulations for outage probability in NOMA-MIMO systems indicate that outage probability decreases with increased transmit power as users get closer to the base station. Our research demonstrates that QC-LDPC codes without $Girth_4$ cycles significantly enhance error correction capabilities and achieve higher spectral efficiency over Rician fading channels. OFDMA-LDPC and SM-NOMA (Spatial Multiplexing-Non Orthogonal Multiple Access) based vehicular communication systems are also compared, emphasizing the impact of 2×2 and 4×4 MIMO configurations on BER and capacity. The results highlight NOMA's superiority and the simplified structure of QC-LDPC, resulting in enhanced system performance in dynamic vehicular communication scenarios. Moreover, increasing the antennas at both ends leads to further performance improvements, with results achieved at a code rate 1/3 among the benchmarked schemes. The Sum-Product algorithm is often employed as a preferred decoding method in high-mobility scenarios due to its efficiency and simplicity, which enhance communication reliability and system capacity. This research also addresses the challenges associated with high vehicle velocities and the resulting Doppler shifts, which are significant in highway and urban scenarios. The mentioned effects were particularly pronounced at a frequency of 0.2 THz and a speed of 120 km/h, impacting signal quality and reliability.

INDEX TERMS V2V communication, NOMA-MIMO, QC-LDPC coding without $Girth_4$, BER, Sum rate, Outage probability, Sum-Product Algorithm.

I. INTRODUCTION

WITHIN the physical layer of 5^{th} generation (5G) wireless communication systems, NOMA has emerged as a crucial technique to facilitate extensive connectivity with minimal latency. It has garnered significant recognition in both the academic and industrial domains. The impending deployment of 5G networks is anticipated to accommodate a substantial number of connections, estimated to reach approximately 100 billion devices, resulting in a rapidly increasing amount of data within a limited spectrum of resources. Among the various techniques used to enhance spectral efficiency, NOMA has recently attracted considerable attention. Although 4G networks support Orthogonal Multiple Access (OMA) to improve BER performance and reduce implementation complexity, it has been found that OMA is suboptimal for spectrum efficiency [1]. The underlying prin-

ciple of NOMA enables the concurrent service of multiple users within the same resource blocks, which is achieved by dividing them into distinct power domains [2]. This design enables NOMA to outperform the OMA techniques, particularly in attaining higher sum rates and lower outage probabilities. This improvement is realized through the deployment of Superposition Coding (SC) at the transmitter and Successive Interference Cancellation (SIC) at the receiver [3].NOMA has recently attracted significant attention from researchers because of its pronounced potential [4]. This innovative approach shows particular promise for enhancing critical communication systems such as vehicle-to-vehicle (V2V) communications, which are crucial in improving road safety and operational efficiency. Vehicular communication facilitates information exchange between vehicles and other objects [5]. The primary objective of vehicular communication is to ensure the safety of traffic and passengers. With heightened expectations in vehicular communities, there is an increasing demand for a more comfortable driving experience and enhanced traffic safety measures. However, the expanding number of vehicles, devices, and services poses challenges to the current communication framework in delivering the expected services at the desired quality. In this context, NOMA's power-domain multiplexing, which enables users to transmit at different power levels, has emerged as a solution to enhance robustness. Therefore, various system models for vehicular communication infrastructure incorporating NOMA have been explored in several studies, and their efficiency has been proven. However, in our study research, we chose to highlight some of these studies, focusing on those most relevant to our investigation. In [6], a cooperative vehicular communication system was proposed that utilized a power-domain downlink NOMA with fixed-gain AF relaying to mitigate severe fading in double Rayleigh fading channels. The performance of the system was evaluated through analytical expressions for outage probabilities and ergodic capacity, considering factors such as transmit power and inter-node distances. The results showed a significant performance compared to the conventional OMA approach. Cooperative NOMA in vehicular communications at intersections was investigated in [7], emphasizing improved performance over OMA by deriving a closed-form outage probability and a quasi-closed-form achievable rate expression. In a closely related study [8], the NOMA-SM technique was introduced as a novel approach for V2V massive MIMO channels to enhance bandwidth efficiency and link reliability, which is highly relevant to our proposed system. The scheme in [9] shows promise for efficient NOMA V2X communication in the Internet of Vehicles, providing insights into its performance with irregular LDPC codes. Furthermore, an analysis of cooperative vehicular communications at intersections using NOMA and a comparison with cooperative OMA were presented in [10]. However, there is a need to evolve a vehicular communication framework to accommodate new technologies and fulfill these heightened expectations. LDPC codes, which are recent channel-coding techniques introduced in New Radio (NR), offer the potential to provide low latency and high reliability for enhanced Vehicle-to-Everything (eV2X) communication. A channel-coding scheme incorporates error detection, error correction, and rate-matching components [11]. It is important to mention that LDPC codes, originally proposed by Gallager [12], had somewhat faded into obscurity owing to computational demands and implementation complexities. However, their significance was reignited in the mid-nineties when researchers such as Mackay and Neal [13] revisited Gallager's work. LDPC codes have demonstrated excellent performance in communication systems. These are linear block codes with a sparse parity-check matrix, allowing for efficient decoding. The LDPC codes exhibited a decoding performance close to the Shannon limit. Additionally, LDPC codes are adopted in the 5G standard by the 3rd Generation Partnership Project (3GPP), acknowledging their high efficiency in correcting errors [14] in transmitted information owing to added noise, interference, or other channel-degrading parameters. The improvement in vehicular system performance was investigated by employing the LDPC channel-coding scheme under various considerations. In [15], the authors investigated multiple decoding methods for LDPC and Polar encoded messages and compared their performance across various channels. The results highlight the effectiveness of LDPC codes in error correction, indicating their suitability for critical communication systems such as V2V, where precise and reliable data transmission is essential for safety and efficiency. Additionally, a PHY layer model that integrates LDPC and MIMO technologies to enhance vehicular communication system performance was proposed in [16]. Simulations using convolutional and various rate LDPC codes were performed for different MIMO configurations. The results demonstrated that the proposed approach achieved over three times higher throughput and a lower BER compared to the conventional approach. While the study in [17] evaluated the performance of error correction coding schemes, including LDPC and Polar codes, in various quality of service (QoS) scenarios, it considered factors such as the minimum Signal-to-Noise Ratio (SNR), transmitted power, maximum range, and throughput for reliability. The study also explored the end-to-end latency, maximum number of vehicles, and vehicle density in each QoS scenario. The authors in [2] presented an enhanced PHY layer for the CV2X standard utilizing LDPC coding and compared it with existing turbo code. The experimental results demonstrated that the proposed LDPC model improved both reliability and throughput while reducing the BER. For inter-vehicle communications, a comparison of coding techniques was presented in [18]. LDPC and QC-LDPC codes outperformed convolutional codes, with QC-LDPC codes demonstrating lower complexity than equivalent LDPC codes, thus achieving a favorable balance between performance and simplicity of implementation. Based on this background, NOMA has demonstrated potential in V2V systems that require high levels of bandwidth efficiency and link reliability. So, it can effectively combine the benefits of

NOMA-MIMO techniques, as suggested in [8], with LDPC coding that is structured algebraically (QC-LDPC without $Girth_4$). This combination aims to enhance vehicular system performance by addressing critical concerns, such as spectral efficiency, interference management, and reliability enhancement. The related compatible technique is considered a valuable contribution to the enhancement of the proposed vehicular system model. The contributions of our study can be summarized as follows:

- The performance of the proposed without clustering vehicular communication system model was evaluated in terms of BER, sum rate, and outage probability through analytical and numerical results. We consider various system parameters, such as the number of transmitted and the received antennas between the transmitter (Alice) and receivers, (Bob_1) and (Bob_2) as: (Alice $\rightarrow$ Bob_1) and (Alice $\rightarrow$ Bob_2) using a specific QC-LDPC rate $(1/3)$.
- Express the upper bound of the BER for near (Bob_1) and far (Bob_2) users in terms of the PEP of the NOMA-MIMO system, supported by the QC-LDPC code. The outage probabilities for both (Bob_1) and (Bob_2) were also expressed in closed forms. These expressions were verified through Monte Carlo simulations.
- The achievable data rate for each user was derived based on Signal-to-Interference-plus-Noise Ratio (SINR) expressions. The final expression for the sum rate, which represents the overall system performance of all NOMA-MIMO/QC-LDPC system users, was also provided.
- Performance of the proposed V2V communication system based on NOMA-MIMO/QC-LDPC techniques compared to other vehicular systems based on SM-NOMA and OFDMA-LDPC.
- The SIC expression is derived by performing ML–Detection at both (Bob_1) and (Bob_2) in the presence of interference from the farthest vehicle to the nearest one. This process is facilitated by the ML-Detection algorithm, which has been demonstrated both theoretically and numerically.
- The structure of the matrices and the process of generating QC-LDPC codes are systematically illustrated. Additionally, we demonstrate the calculation of the minimum distance in the absence of four cycles in their Tanner graphs and explore the growth of minimum instances with block length. This generation is outlined as an algorithm in our study. These characteristics are important when evaluating the effectiveness of error-correcting codes in vehicular environments.
- The demonstration of channel vector extraction for both close (Bob_1) and distant (Bob_2) users from the channel matrix is a valuable addition to our research. By expanding the number of transmitted and received antennas, we can extract individualized channel vectors for each user from the MIMO channel matrix, based on their respective distances from the transmitter.

Our numerical results verify the improvement of the system in terms of the BER and sum rate for both near and far users. The amount of enhancement that can be achieved depends on the MIMO configuration and coding rate of the QC-LDPC code, which is defined as the ratio of the number of information bits to the total number of bits transmitted.

A. NOTATION

Upper and lower-case bold characters indicate the matrices and vectors, respectively. $(.)^{-1}$,$(.)^{H}$ and $[.]_{p,q}$ represent the inverse, conjugate-transpose and entry in the p^{th} row and q^{th} column of the matrix, respectively. $E_x.$ indicates the expectation of the random variable x. $\mathbf{M} \in \mathbb{C}^{A\times B}$: is a complex-element matrix with A row and B column. I_A, denotes the identity matrix with A row and A column.$\|.\|$ denotes the Euclidean norm of a vector.

The remainder of this paper is organized as follows. In Section II, we present the system model of the NOMA-MIMO/QC-LDPC. Section III provides an overview of Propagation with Rician Channel. Challenges in current vehicular communication systems are outlined in Section IV as Problem Formulation, followed by the Proposed Solution in Section V. Section VI provides an in-depth exploration of the adopted QC-LDPC coding scheme. The analyses of the Error Performance and SINR for our proposed system are presented in Sections VII and VIII, respectively. Finally, Section IX concludes by summarizing the results and discussions based on the obtained findings. For convenience, we have listed the most frequently used notations.

II. SYSTEM MODEL

As depicted in Fig.1, the NOMA-MIMO/QC-LDPC approach was implemented for both transmission links: $(Alice{\rightarrow}Bob_2)$ with a distance represented as d_{A-B_2} and $(Alice{\rightarrow}Bob_1)$ with a distance denoted as d_{A-B_1}. At $(Alice)$, two independent bit streams are prepared for transmission. The first N-bit streams for (Bob_2) and the others for (Bob_1), employ superposition coding using the NOMA technique [6].

$$\mathbf{x}_{\text{NOMA/QC-LDPC}} = \sqrt{P_t}\left(\sqrt{\alpha_{b_1}}\,\mathbf{xc}_{b_1} + \sqrt{\alpha_{b_2}}\,\mathbf{xc}_{b_2}\right) \qquad (1)$$

Subsequently, $\text{xc}_{b_1 n} \in [\text{xc}_{b_1 1} : \text{xc}_{b_1 N}]$ and $\text{xc}_{b_2 n} \in [\text{xc}_{b_2 1} : \text{xc}_{b_2 N}]$ are intended to be encoded-modulated symbols that can be used for $(Alice \rightarrow \text{Bob}_1)$ and $(Alice{\rightarrow}Bob_2)$ transmissions respectively. A block of $(N-M)$ information bits is first encoded by a QC-LDPC encoder that produces a code word with a length of N coded bits with M redundant bits. The coded bits $\mathbf{xc}_{b_1}$ and $\mathbf{xc}_{b_2} \in \{0,1\}$ are passed to a Binary Phase-Shift-Keying (BPSK) modulator. The output of the modulator is given by $\mathbf{xc}_{b_1} = (-1)^{\mathbf{xc}_{b_1}} \in \{+1,-1\}$ and $\mathbf{xc}_{b_2} = (-1)^{\mathbf{xc}_{b_2}} \in \{+1,-1\}$. Considering P_t as the total transmitted power at $(Alice)$, the allocated powers for near and far users depend on α_{b_1} and α_{b_2} which [6] are denoted as power allocation coefficients for the mentioned users, respectively under the assumption that $d_{A-B_2} \geq d_{A-B_1}$. According to the principle of NOMA, the transmitted power for the distant user (Bob_2) must be higher than that of the

closest one (Bob_1) which has a good channel condition. Therefore, the coefficients for the receivers should satisfy $\alpha_{b_1} + \alpha_{b_2} = 1$ with $\alpha_{b_2} > \alpha_{b_1}$. Moreover, it is approximated that the average energy per transmission at $(Alice)$ is equal to one satisfying, $E\{|\mathbf{xc}_{b_1}|^2\} = E\{|\mathbf{xc}_{b_2}|^2\}$. The complex symbol $\sqrt{\alpha_{b_1}}\mathbf{xc}_{b_1} + \sqrt{\alpha_{b_2}}\mathbf{xc}_{b_2}$ can then be transmitted using a V2V-MIMO channel [19]. In the proposed system, the channel matrix for the two transmission links is defined as $\mathbf{H}_{\text{MIMO}} \in \mathbb{C}^{N_r \times N_t}$. Considering that all entries of the channel matrix are independent and identically distributed $(i.i.d)$ with a $\mathcal{CN}(0,1)$ while the complex fading envelopes between the transmitter and both receivers are derived from $\mathbf{H}_{\text{MIMO}}$ under the condition that the gains of both (Bob_1) and (Bob_2) are arranged such that $|\mathbf{h}_{b_1}|^2 \geq |\mathbf{h}_{b_2}|^2$. In addition, it is assumed that the full Channel State Information at the Receivers (CSIR) and perfect synchronization for the channel vectors are described in terms of both time and frequency as in [3], [6]. The approach to extracting the column vector $\mathbf{h}_{b_1} \in \mathbb{C}^{N_r \times 1}$ with the highest gain from $\mathbf{H}_{\text{MIMO}} \in \mathbb{C}^{N_r \times N_t}$ is considered by using the 1-norm for columns, which is calculated by finding the maximum absolute column sum among all columns of matrix $\mathbf{H}_{\text{MIMO}}$ as in the following equation [20]:

$$\|\mathbf{H}_{\text{MIMO}}\|_1 = \max_{j=1,\ldots,N_t} \sum_{i=1}^{N_r} |\mathbf{H}_{\text{MIMO}} ij| \tag{2}$$

where $\|\mathbf{H}_{\text{MIMO}}\|_1$ represents 1-norm. Based on (2), column index j indicates that the column with the highest gain can be expressed as follows:

$$\arg\max_{j} \left(\sum_{i=1}^{N_r} |\mathbf{H}_{\text{MIMO}} ij| \right) \tag{3}$$

Thus, the mentioned column vector can be retrieved as $\mathbf{h}_{b_1} = \mathbf{H}_{\text{MIMO}}(:, j)$ whereas the other column vector with the lowest channel gain is allocated for the farthest user as $\mathbf{h}_{b_2} \in \mathbb{C}^{N_r \times 1}$. For (Bob_1) the copy of $\mathbf{x}_{\text{NOMA/QC-LDPC}}$ is sent through channel $\mathbf{h}_{b_1} \in \mathbb{C}^{N_r \times 1}$ and it is supposed to be received, as in the following expression:

$$\mathbf{y}_{b_1} = \sqrt{d_{A-B_1}^{-\eta}} \sum_{i=1}^{N_r} \mathbf{h}_{b_1}(i) \mathbf{x}_{\text{NOMA/QC-LDPC}} + \mathbf{w}_{b_1} \tag{4}$$

It can then be expanded by substituting (1) into (4) as follows:

$$\begin{aligned} \mathbf{y}_{b_1} &= P_{d_{(A-B_1)|B_1}} \left(\sum_{i=1}^{N_r} \mathbf{h}_{b_1}(i) \cdot \mathbf{x}_{b_1} \right) \\ &+ P_{d_{(A-B_1)|B_2}} \left(\sum_{i=1}^{N_r} \mathbf{h}_{b_1}(i) \cdot \mathbf{x}_{b_2} \right) + \mathbf{w}_{b_1} \end{aligned} \tag{5}$$

where: $P_{d_{(A-B_1)|B_1}} = \sqrt{P_t \cdot d_{A-B_1}^{-\eta} \cdot \alpha_{b_1}}$ and $P_{d_{(A-B_1)|B_2}} = \sqrt{P_t \cdot d_{A-B_1}^{-\eta} \cdot \alpha_{b_2}}$ represent the desired received power for (Bob_1) and the interference power for (Bob_2) at (Bob_1) respectively. Meanwhile, for (Bob_2) the copy of $\mathbf{x}_{\text{NOMA/QC-LDPC}}$ is sent through channel $\mathbf{h}_{b_1}$ and is supposed to be received as in the following expression:

$$\mathbf{y}_{b_2} = \sqrt{d_{A-B_2}^{-\eta}} \sum_{i=1}^{N_r} \mathbf{h}_{b_2}(i) \mathbf{x}_{\text{NOMA/QC-LDPC}} + \mathbf{w}_{b_2} \tag{6}$$

At the far user (Bob_2), the received signal after decoding it at (Bob_2) can be expanded by substituting (1) into (6):

$$\begin{aligned} \mathbf{y}_{b_2} &= P_{d_{(A-B_2)|B_2}} \left(\sum_{i=1}^{N_r} \mathbf{h}_{b_2}(i) \cdot \mathbf{xc}_{b_2} \right) \\ &+ P_{d_{(A-B_2)|B_1}} \left(\sum_{i=1}^{N_r} \mathbf{h}_{b_2}(i) \cdot \mathbf{xc}_{b_1} \right) + \mathbf{w}_{b_2} \end{aligned} \tag{7}$$

where: $P_{d_{(A-B_2)|B_2}} = \sqrt{P_t \cdot d_{A-B_2}^{-\eta} \cdot \alpha_{b_2}}$ and $P_{d_{A-B_2|B_1}} = \sqrt{P_t \cdot d_{A-B_2}^{-\eta} \cdot \alpha_{b_1}}$ represent the dominant received power at (Bob_2) and the low power for (Bob_1) signal which is indicated at (Bob_2) respectively. Where η denotes the path-loss exponent. The vectors $\mathbf{w}_{b_1}$ and $\mathbf{w}_{b_2}$ represent the complex additive white Gaussian noise (AWGN) following the distributions $\mathcal{CN}(0, \sigma^2)$. NOMA leverages SIC to decode signals in a shared time and frequency environment. In SIC, signals from high-power users are first eliminated, and lower-power signals are treated as noise. Consequently, (Bob_1)'s post-SIC signal is as defined in [8], both (Bob_2) and (Bob_1) must first detect Bob_2's signal, using the optimal Maximum Likelihood (ML) detector, as detailed in equations (8) and (9), respectively:

$$\hat{\mathbf{xc}}_{b_2} = \text{argmin} \, \|\mathbf{y}_{b_2} - P_{d_{(A-B_2)|B_2}} \left(\sum_{i=1}^{N_r} \mathbf{h}_{b_2}(i) \cdot \mathbf{xc}_{b_2} \right) \|^2 \tag{8}$$

Eliminating the interface imposed by (Bob_2) on $\mathbf{y}_{b_1}$ and Performing another ML detection to acquire $\hat{\mathbf{xc}}_{b_1}$

$$\hat{\mathbf{xc}}_{b_1} = \text{argmin} \, \|\mathbf{y}_{b_1\text{-clean}} - P_{d_{(A-B_1)|B_1}} \left(\sum_{i=1}^{N_r} \mathbf{h}_{b_1}(i) \cdot \mathbf{xc}_{b_1} \right) \|^2 \tag{9}$$

It is possible to provide the specifics of the steps required to implement the proposed system, as outlined in **Procedure (1)**.

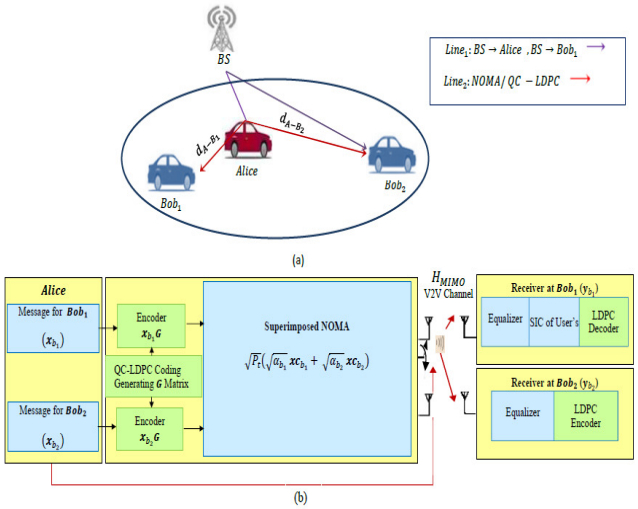

FIGURE 1: a. Proposed System Model, b. Block Diagram of the Model

III. PROPAGATION WITH RICIAN CHANNEL

Due to distinct propagation conditions, V2V channels display contrasting propagation characteristics when compared to cellular communication channels. In V2V communications, both the transmitter and receiver operate at lower levels and are encompassed by numerous scatters that induce substantial Doppler shifts, rendering the channel non-stationary [21]. In this study, we investigate a spatial-temporally correlated Rician channel model as previously employed in [8] and [22] to characterize our narrow-band V2V massive MIMO channel. The model accommodates realistic obstacles and diverse channels, and aligns with wireless standards, directly balancing line-of-sight and multi-path fading in complex vehicular environments.

Therefore, for a Rician fading MIMO channel, the $N_r \times N_t$ matrix of channel $\mathbf{H}_{\text{MIMO}}$ is defined as follows: [23], [24].

$$\mathbf{H}_{\text{MIMO}} = \sqrt{\frac{K}{K+1}}\mathbf{H}_{\text{LoS}} + \sqrt{\frac{1}{K+1}}\mathbf{H}_{\text{NLoS}} \tag{10}$$

where K is the channel rice factor, which can be defined as the ratio of P_{LoS} to P_{NLoS} ($K = \frac{P_{\text{LoS}}}{P_{\text{NLoS}}}$). The correlation matrix of $\mathbf{H}_{\text{NLoS}}$ is then given by:

$$R_{\mathbf{H}_{\text{NLoS}}} = \mathbb{E}\{\mathbf{H}_{\text{NLoS}}^{\text{H}}\mathbf{H}_{\text{NLoS}}\} = N_r I_{N_t} \tag{11}$$

where $[\mathbf{H}_{\text{LoS}}]_{vw} = h_{\text{LoS}}(v,w)$, for all channel coefficient pairs $(h_{\text{LoS}}(v,w) \quad , h_{\text{LoS}} \quad (\hat{v},\hat{w}))$ $(v,\hat{v} \in \{1:N_t\})$ and $(w,\hat{w} \in \{1:N_r\})$. As assumed in [22]:

$$\mathbb{E}[h_{\text{LoS}}(v,w)^R h_{\text{LoS}}(\hat{v},\hat{w})^R] = \mathbb{E}[h_{\text{LoS}}(v,w)^{\text{I}} h_{\text{LoS}}(\hat{v},\hat{w})^{\text{I}}],$$
$$\mathbb{E}[h_{\text{LoS}}(v,w)^R h_{\text{LoS}}(\hat{v},\hat{w})^{\text{I}}] = \mathbb{E}[h_{\text{LoS}}(v,w)^{\text{I}} h_{\text{LoS}}(\hat{v},\hat{w})^R] = 0$$

This implies that the real and imaginary parts have identical auto-correlations and no correlation exists between them. Hence, the entries of the channel matrix $\tilde{\mathbf{H}}$ are characterized using the Kronecker correlation model [22], [24], where:

$$\mathbf{H}_{\text{NLoS}} = \sum_{p}^{\frac{1}{2}} \tilde{\mathbf{H}} \sum_{q}^{\frac{1}{2}T} \tag{12}$$

where $\sum_q \in C^{N_t \times N_t}$ and $\sum_p \in C^{N_r \times N_r}$ are the real-valued and Hermitian symmetric matrices, at transmitter $(Alice)$ and receiver (Bob_2), respectively. Such correlation matrices are defined by their elements as: $[\sum_q]_{v,v'} = \sigma^q_{v,v'}$, for $v,v' \in \{1:N_t\}$ and $[\sum_p](w,\hat{w}) = \sigma^p_{(w,\hat{w})}$, for $w,w' \in \{1:N_r\}$. Matrix $\tilde{\mathbf{H}}$ represents the Rayleigh fading channel, with its elements depicted as independent and identically distributed complex Gaussian random variables $[\tilde{\mathbf{H}}]_{vw} = \tilde{h}_{(v,w)} \sim \mathcal{CN}(0,1)$. The time-varying nature of the V2V channel is considered through the temporal correlation, denoted as $\delta(\tau)$ which expresses the expectation between the channel matrices at time instances t and $t+\tau$, defined as $\delta(\tau) = \mathbb{E}\{(t)\tilde{\mathbf{H}}(t+\tau)\}$. The temporal correlation utilizes the Jakes' model from [25], expressed as $\delta(\tau) = J_0(2\pi f_D \tau)$, where f_D signifies the maximum Doppler frequency associated with the carrier frequency and terminal velocity.

The Rician distribution emerges as a special instance of Rayleigh distribution when the dominant component is disregarded [26]. Consequently, the magnitudes of the matrix $\mathbf{H}_{\text{MIMO}}$ elements' adhere to the subsequent Rician probability density function (pdf) [24]:

$$f_R(r) = 2(1+K)re^{-(1+K)^{r^2}-K} J_0\left(2\sqrt{K(1+K)}\,r\right) \tag{13}$$

where J_0 is the modified Bessel function of the first order zero. The Rayleigh channel typically lacks Line-of-Sight (LOS). However, certain channels incorporate the LOS signal through various paths, including the direct path, resulting in a notably stronger LOS signal than that received by others. This scenario is captured by Rician fading, characterized by an amplitude gain following a Rician distribution [26].

Procedure (1): Perform SIC and ML – Detection

Inputs: N total size of each: **symbol** $_{(A\to B_2)}$, **symbol** $_{(A\to B_1)}$, and **symbol** $_{(B_2\to B_1)}$.

Procedure:

1: ML–Detection superimposed on NOMA/QC-LDPC encoded-modulated symbols.

2: Enumerate all possible NOMA/QC-LDPC transmitted-encoded symbol combinations in the proposed system.

3: Calculate the transmitted symbols for (Bob_1):

$$\underset{(A\to B_1)}{\textbf{symbol}} = P_{d_{(A-B_1)|B_1}}\left(\sum_{i=1}^{N_r} \mathbf{h}_{b_1}(i)\cdot \mathbf{xc}_{b_1}\right).$$

4: Calculate the transmitted symbols for (Bob_2):

$$\underset{(A\to B_2)}{\textbf{symbol}} = P_{d_{(A-B_2)|B_2}}\left(\sum_{i=1}^{N_r} \mathbf{h}_{b_2}(i)\cdot \mathbf{xc}_{b_2}\right).$$

5: Calculate the interfering symbols from (Bob_2) to (Bob_1):

$$\underset{(A\to B_1)}{\textbf{symbol}} = P_{d_{(A-B_1)|B_2}}\left(\sum_{i=1}^{N_r} \mathbf{h}_{b_1}(i)\cdot \mathbf{xc}_{b_2}\right).$$

6: Detect the interfering symbols as $\mathbf{xc}_{b_2-\text{detected}}$ by computing the minimum Euclidean distances between $\mathbf{y}_{b_1}$ and **symbol** $_{(B_2\to B_1)}$ as:

$$\text{argmin}\|\mathbf{y}_{b_1} - P_{d_{(A-B_1)|B_2}}\left(\sum_{i=1}^{N_r} \mathbf{h}_{b_1}(i)\cdot \mathbf{xc}_{b_2}\right)\|^2.$$

7: Eliminate the interference imposed by $\mathbf{xc}_{b_2-\text{detected}}$ on $\mathbf{y}_{b_1}$ by calculating $\mathbf{y}_{b_1-\text{clean}}$ as follows:

$$\mathbf{y}_{b_1} - P_{d_{(A-B_1)|B_2}}\left(\sum_{i=1}^{N_r} \mathbf{h}_{b_1}(i)\cdot \mathbf{xc}_{b_2-\text{detected}}\right)$$

8: Repeat step (6) for $\mathbf{xc}_{b_1}$ on $\mathbf{y}_{b_1-\text{clean}}$ and set the detected encoded-modulated symbols $\hat{\mathbf{x}}, \mathbf{c}_{b_1}$ at (Bob_1), as it was calculated in (9) :

$$\text{argmin}\|\mathbf{y}_{b_1-\text{clean}} - P_{d_{(A-B_1)|B_1}}\left(\sum_{i=1}^{N_r} \mathbf{h}_{b_1}(i)\cdot \mathbf{xc}_{b_1}\right)\|^2.$$

9: Find the minimum Euclidean distance between $\mathbf{y}_{b_2}$ and **symbol** $_{(A\to B_2)}$ and set the detected symbols $\hat{\mathbf{xc}}_{b_2}$ as in (8):

$$\text{argmin}\|\mathbf{y}_{b_2} - P_{d_{A-B_2|B_2}}\left(\sum_{i=1}^{N_r} \mathbf{h}_{b_2}(i)\cdot \mathbf{x}_{b_2}\right)\|^2.$$

End-Procedure

IV. EXTRACTION OF CHANNEL VECTORS FROM H_{MIMO} MATRIX

Due to the expansion of the number of users in the system, the number of transmitted and received antennas has also increased. For our proposed system based on NOMA technology, the channel $\mathbf{h}_{b_i} \in \mathbb{C}^{N_r \times 1}$ for each user (Bob_i), where $i \in \{1 : N_r\}$ should be extracted from the channel matrix $\mathbf{H}_{\text{MIMO}} \in \mathbb{C}^{N_r \times N_t}$ based on their distances d_{A-B_i}, as shown in (2) and (3), respectively. Suppose, $d_{A-B_{N_r}} > d_{A-B_{N_r-1}} > \cdots > d_{A-B_1}$ and $|\mathbf{h}_{b_{N_r}}|^2 \leq |\mathbf{h}_{b_{N_r-1}}|^2 \leq \cdots \leq |\mathbf{h}_{b_1}|^2$. Therefore, the channel column vector for each user is extracted as follows:

$$\|\mathbf{h}_{b_i}\|^2 \propto \frac{1}{d_{A-B_i}} \tag{14}$$

Then, the superimposed encoded-modulated signal transmitted by $(Alice)$ can be represented as:

$$\mathbf{x}_{\text{NOMA/QC-LDPC}} = \sqrt{P_t}\left(\sum_{i=1}^{N_r} \sqrt{\alpha_{b_i}}\, \mathbf{xc}_{b_i}\right) \tag{15}$$

Here, $\mathbf{xc}_{b_i}$ represents a block of N information bits corresponding to the encoded-modulated transmitted symbols between $(Alice)$ and (Bob_i) and α_{b_i} denotes the power allocation coefficients. These coefficients must satisfy $\sum_{i=1}^{N_r} \alpha_{b_i} = 1$, as illustrated previously in the System Model section, but specifically for the two users, (Bob_1) and (Bob_2). The selection of power allocation coefficients plays a crucial role in determining the performance of a NOMA network. They should be ordered according to the extracted channel vectors, as follows:

$$\|\mathbf{h}_{b_i}\|^2 \propto \frac{1}{\alpha_{b_i}} \tag{16}$$

Therefore, the coefficient assigned to the farthest user (Bob_{N_r}) which is characterized by the weakest channel gain should exceed that of the other users. Conversely, the nearest user (Bob_1) should have the lowest coefficient, followed by others in a similar pattern as $\alpha_{b_{N_r}} > \alpha_{b_{N_r-1}} > \cdots > \alpha_{b_1}$. After sending the copy of $\mathbf{x}_{\text{NOMA/QC-LDPC}}$ through the extracted channel vectors $\mathbf{h}_{b_i} \in \mathbb{C}^{N_r \times 1}$, the resulting signal received at each user (Bob_i) is represented as indicated in (4) and (6):

$$\mathbf{y}_{b_i} = \sqrt{d_{A-B_i}^{-\eta}} \sum_{k=1}^{N_r} \mathbf{h}_{b_i}(k) \cdot \mathbf{x}_{\text{NOMA/QC-LDPC}} + \mathbf{w}_{b_i} \tag{17}$$

At the i^{th} Bob, SIC is employed to remove users allocated with higher power levels, treating users with lower power allocations as noise. Consequently, SIC is executed $(N_r - i)$ times at (Bob_i).Thus, the signal at the i^{th} Bob user which posts the SIC process, can be represented as follows :

$$\hat{\mathbf{y}}_{b_i} = \mathbf{y}_{b_i} - \left(\sqrt{P_t d_{A-B_i}^{-\eta}} \sum_{k=1}^{N_r} \mathbf{h}_{b_i}(k)\right)\left(\sum_{j=i+1}^{N_r} \sqrt{\alpha_{b_j}} \cdot \mathbf{xc}_{b_j}\right) \tag{18}$$

Ultimately, determining the user's transmitted symbol is accomplished by utilizing maximum likelihood estimation (MLE). The ascertained symbol for (Bob_i) is formally expressed in (8), (9) as follows:

$$\hat{\mathbf{xc}}_{b_i} = \arg\min \left\| \mathbf{y}_{b_i} - P_{d_{A-B_i|B_i}} \left(\sum_{k=1}^{N_r} \mathbf{h}_{b_i}(k) \cdot \hat{\mathbf{xc}}_{b_i} \right) \right\|^2 \tag{19}$$

where the transmitted symbols $\mathbf{xc}_{b_i}$ of N information bits are encoded first by the QC-LDPC and then modulated considering BPSK as a modulated scheme for (Bob_i). The SIC decoding procedure for a system of N_r users is illustrated in Fig.2. As observed in the mentioned figure, the steps of SIC procedures increase owing to the increasing number of MIMO configurations.

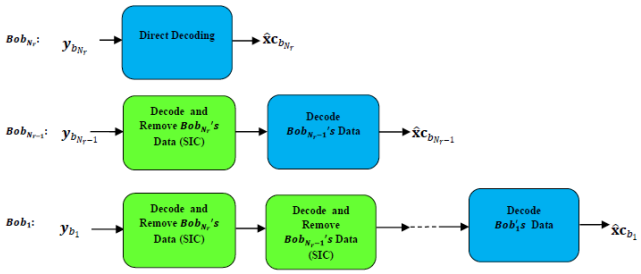

FIGURE 2: Illustrates the SIC decoding procedure for a system of N_r users.

V. PROBLEM FORMULATION

Our proposed system addresses the challenges identified in other vehicular communication systems, specifically those in [8] and [16], which encounter challenges related to dynamic channel conditions, high mobility, and varying interference levels. To improve the BER performance and sum rate in such scenarios, it is important to summarize the challenges in other systems. The primary challenge addressed in [8] revolves around its handling of Spatial-Multiplexing (SM), which leads to an increase in BER owing to difficulties in managing channel variation, restricted spatial diversity, and complexities in resource allocation. Where the Spatial-Domain Capacities are calculated using the formula (6) & (10) in [8] in terms of the Mutual Information (MI) conveyed by the spatial-domain Transmit Antenna (TA) constellations depending on the probability density function (PDF) of the channel output $(\mathbf{y}_V)$, received over the i^{th} channel vector of $\mathbf{H}$, for far user as:

$$P_r(\mathbf{y}_V|\mathbf{h}_i) = \frac{1}{\pi^{N_r} \det(\Sigma_i)} \exp\left\{-\mathbf{y}_V^H \Sigma_i^{-1} \mathbf{y}_V\right\} \quad [8, \text{Equ.6}]$$

While for the near user, the PDF of the channel output $\mathbf{y}_U$ received over the i^{th} channel vector of $\mathbf{G}$, given by:

$$P_r(\mathbf{y}_U|\mathbf{g}_i) = \frac{1}{\pi^{N_u} \det(\Omega_i)} \exp\left\{-\mathbf{y}_U^H \Omega_i^{-1} \mathbf{y}_U\right\} \quad [8, \text{Equ.10}]$$

Furthermore, the challenge of considering SM can be pointed out as the assumption of equiprobable activation of antennas, which might not guarantee an optimal spatial design. The

other related system [16] was based on OFDMA-MIMO techniques and was supported by LDPC codes. It is mentioned that the performance of LDPC varies with the coding rates, using coding rates higher than 1/2 is drastically worse than that when coding rates are considered 1/2 and lower. The choice between low and high code rates involves trade-offs between error performance, spectral efficiency, system capacity, and complexity. However, NOMA outperforms (Orthogonal Frequency Division Multiple Access) in vehicular communication systems, because of its ability to effectively handle diverse user requirements by ensuring optimal resource utilization and resilience against interference.

VI. PROPOSED SOLUTION

We propose a compact system that integrates NOMA-MIMO advantages with the simpler structure of QC-LDPC, excluding Girth_4 codes in LDPC to improve hardware compatibility, which will enhance our vehicular system model in terms of BER and sum rate. The absence of Girth_4 cycles in the Tanner graph of QC-LDPC codes offers an advantage, especially in higher signal-to-noise ratio (SNR) scenarios. This absence enhances the error-correction performance, particularly in addressing the error floor effects often seen in LDPC codes containing short cycles. It effectively defines an error floor as a scenario where the BER stabilizes at a non-zero value despite an increase in the SNR. The mention of this issue being challenging in high-speed communication systems and demanding channel conditions provides a context for why mitigating error floors is crucial for ensuring the system's reliability and efficiency. However, unlike traditional LDPC codes which may require specific code rate designs for optimal performance, QC-LDPC codes offer advantages that make them suitable for various code rates. In the proposed system, the utilization of NOMA techniques in combination with QC-LDPC codes at lower rates can improve the overall spectral efficiency by facilitating more reliable communication and reducing the need for retransmissions or additional overhead for error control.

VII. QC-LDPC CODING SCHEME

High-quality QC-LDPC codes exhibit an algebraic structure, featuring substantial minimum distances and strong performance in terms of BER. They rely on index matrices that determine the shifts of circulating sparse parity-check matrices [18], imparting QC characteristics that can enhance the encoder efficiency. In addition, the code's algebraic structure enables high-speed and efficient Very Large-Scale Integration (VLSI) implementation. Several LDPC code design methods employ random construction, which leads to challenges in managing large parity-check matrices, data encoding, and performance analysis owing to the lack of structure. The introduction of an algebraic structure can help to address these issues. However, the performance of QC-LDPC code in terms of girth, distance, and BER does not match that of random codes [18], [27].

A. DESIGN OF PARITY CHECK MATRIX OF QC-LDPC WITHOUT $GIRTH_4$ [27], [28]

Utilizing the framework of multiplicative groups involves integrating circulate matrices into a parity-check matrix to construct systematic QC-LDPC block codes with diverse block lengths and rates. In the context of prime number q, the integers within the set $\{0, \ldots, q-1\}$ collectively create a field where both addition and multiplication are performed modulo q, forming the Galois field $GF(q)$. Within this field, non-zero elements establish a cyclic multiplicative group. Consider two non-zero elements, a and b, each with their respective multiplicative orders, denoted as $O(a)$ and $O(b)$. Such elements exist if both k and j are divisors of $O(q)$, where $O(q) = q-1$ represents the multiplicative group order. Define a $k \times j$ index matrix $\mathbf{P}$ of elements from GF(q), which has its $(s,t)^{\text{th}}$ element $P_{s,t} = a^t b^s$ as follows:

$$\mathbf{P} = \begin{bmatrix} 1 & \cdots & a^{(j-1)} \\ \vdots & \ddots & \vdots \\ b^{(k-1)} & \cdots & a^{(j-1)}b^{(k-1)} \end{bmatrix} \tag{20}$$

Where $0 \leq s \leq k-1$ and $0 \leq t \leq j-1$. The circulating sub-matrix at the (s,t) position in matrix $\mathbf{H}$ is created by cyclically moving the rows of the identity matrix to the left by $\mathbf{P}_{(s,t)}$ positions. This process results in a binary parity-check matrix with dimensions $(M \times N)$, implying that the corresponding code has a rate $(R \geq 1 - k/j)$. Here, $M = kq$ and $N = jq$. Then, $\mathbf{H} \in \mathbb{Z}_2^{(M \times N)}$ is made up of a $(k \times j)$ array of circular sub- matrices as shown in the following:

$$\mathbf{H} = \begin{bmatrix} I_1 & \cdots & I_{a^{(k-1)}} \\ \vdots & \ddots & \vdots \\ I_{b^{(j-1)}} & \cdots & I_{a^{(k-1)}b^{(j-1)}} \end{bmatrix} \tag{21}$$

where $\mathbf{I}_x$ is a $q \times q$ identity matrix with rows shifted to the left by x positions. By construction, each column of the matrix $\mathbf{H}$ contains k columns and every row contains j columns where $\mathbf{H}$ represents an (N, k, j) regular LDPC code. The codes developed using this method exhibit QC property with a period of j. Consequently, shifting a codeword by one position within each of the j blocks of circulating sub-matrices yields a different codeword. The suggested code construction produces a series of codes in which the minimum distances increase proportionally with block length N. The procedure for determining the minimum distance of QC codes is outlined as follows:

$$\mathbf{H} = [\mathbf{A} \quad \vdots \quad \mathbf{B}]_{(M \times N)} \tag{22}$$

$$\mathbf{H} = \begin{bmatrix} a_{11} & \cdots & a_{1M} & b_{1(M+1)} & \cdots & b_{1N} \\ \vdots & \ddots & \vdots & \vdots & \ddots & \vdots \\ a_{M1} & \cdots & a_{MM} & b_{M(M+1)} & \cdots & b_{MN} \end{bmatrix}_{(M \times N)} \tag{23}$$

where $\mathbf{A} \in \mathbb{Z}_2^{(M \times M)}$ and $\mathbf{B} \in \mathbb{Z}_2^{(M \times (N-M))}$. The generator matrix $\mathbf{G} \in \mathbb{Z}_2^{(M \times N)}$ can be constructed from $\mathbf{H}$

by calculating $\mathbf{A}^{-1} \in \mathbb{Z}_2^{(M\times M)}$ and combining it with $\mathbf{B} \in \mathbb{Z}_2^{(M\times(N-M))}$ as follows:

$$\mathbf{D} = \left[\mathbf{A}^{-1} \otimes \mathbf{B}\right]_{M\times(N-M)} \tag{24}$$

The systematic form of the generator matrix can be represented as follows:

$$\mathbf{G} = [\mathbf{D}^{-1} \quad \vdots \quad \mathbf{I}]_{M\times N} \tag{25}$$

where $\mathbf{D}^{-1} \in \mathbb{Z}_2^{(N-M)\times M}$ and $\mathbf{I} \in \mathbb{Z}_2^{M\times M}$, and set the maximum number of iteration is set to $\text{Iter}_{\max}$. In our study, the transmitted symbols $\mathbf{x}_{b_1}$ and $\mathbf{x}_{b_2}$ are encoded by the QC-LDPC encoder as $\mathbf{xc}_{b_1}$ and $\mathbf{xc}_{b_2}$ of length N, respectively:

$$\mathbf{xc}_{b_1} = \mathbf{x}_{b_1} \cdot \mathbf{G} \tag{26}$$

$$\mathbf{xc}_{b_2} = \mathbf{x}_{b_2} \cdot \mathbf{G} \tag{27}$$

where $\mathbf{x}_{b_1} = [\mathrm{x}_{b_1 1} : \mathrm{x}_{b_1(N-M)}]$ and $\mathbf{x}_{b_2} = [\mathrm{x}_{b_2 1} : \mathrm{x}_{b_2(N-M)}]$ are symbols for the random information bit vectors of length $(N-M)$, generated from $(Alice)$ for (Bob_1) and (Bob_2) respectively. To obtain high SNRs, the maximum-likelihood decoding performance of an error-correcting code should be dominated by the minimum distance of the code. After performing the encoded symbols $\mathbf{xc}_{b_1}$ and $\mathbf{xc}_{b_2}$ produce another coded symbol $\mathbf{x}'c_{b_1}$ and $\mathbf{x}'c_{b_2}$ of length N are used for (Bob_1) and (Bob_2) respectively. Next, compute the distance between the two binary vectors $d(\mathbf{xc}_{b_1}, \mathbf{x}'c_{b_1})$ and $d(\mathbf{xc}_{b_2}, \mathbf{x}'c_{b_2})$ and record the minimum value of the results as $d_{\min}$. The calculation of other distance values is repeated, the obtained results are compared, and the last calculated minimum value $d_{\min}$ until the maximum specified number of iterations $\text{Iter}_{\max}$. The procedures for constructing the **G** and **H** matrices can be followed according to the Algorithm 1. Matrices **G** and **H** are defined as the generator and parity-check matrices, respectively, used for encoding and decoding the transmitted and received symbols, respectively

B. DEFINITIONS OF CYCLES WITH AND WITHOUT $GIRTH_4$

The LDPC codes use a soft-decision decoding algorithm that preserves the received magnitude of each bit. This algorithm can be described more easily using a graphical representation of the parity-check matrix $\mathbf{H} = [\mathbf{h}_{ij}]_{0\le i<M, 0\le j<N}$ called a Tanner graph where i^{th} Check Node is connected to the j^{th} Variable Node by an edge if and only if $h_{ij} = 1$. Fig.3 shows an example of the QC-LDPC of a rate $(1/2)$ [27].

In a Tanner graph, a cycle denotes a finite group of interconnected edges where each edge originates and concludes at the same node, and it meets the requirement that no node (excluding the initial and final nodes) is visited more than once [29]. The length of a cycle is simply the count of its edges. The girth of a Tanner graph (g) is characterized as the length of the shortest even cycle with a minimum length of four, which is denoted as $\mathrm{Girth}_4(p_1, p_2, p_3, p_4)$. This is illustrated in Fig. 4 [30], where the positions of 1's are denoted as (p_1, p_3) in variable edge V_a belonging to the Check Nodes $(C_a \& C_b)$, and the other related positions are denoted as (p_2, p_4) in variable edge V_b belonging to the Check Nodes $(C_a \& C_b)$ .If the configuration depicted in Fig. 4 is absent from the parity-check matrix, then there are no cycles of length 4 in the LDPC code that is lengths $L(p_1, p_3) \neq L(p_2, p_4)$ [30]. The benefits of the QC-LDPC code segment include ensuring that the parity check matrix **H** is represented as a sparse matrix, especially when it's not already sparse. This can be particularly useful when dealing with large matrices with many zero elements because using sparse representation can save memory and computational resources .

Algorithm 1 : An Algebraic Construction of a QC-LDPC Matrix

. **Procedure:** Construction of circulate sub-matrices within the parity-check matrix **H**.

Require: Size of Galois Field $GF(q)$, number of check nodes k, number of variable nodes j, design parameters for the index matrix **P** (a and b) with specific multiplicative orders.

Ensure: parity check & generator matrices for the QC-LDPC code.

Create the $k \times j$ index matrix **P** using elements a and b.
Set $\mathbf{P}[j,k] = 0$
for $s = 1$ to k **do**
  for $t = 1$ to j **do**
    Calculate the element in the index matrix: $\mathbf{P}[s,t] = \mod (a^{(s-1)}b^{(t-1)}, q)$.
  end for
end for
Create a circulate sub-matrix by cyclically shifting the rows of the identity matrix.
% Initialize the size of the parity-check matrix
$M = k \times p$
$N = j \times p$
% Initialize the parity-check matrix **H**
$\mathbf{H} = \text{zero}(M, N)$
for $s = 1$ to k **do**
  for $t = 1$ to j **do**
    sub-matrix = circshift(eye(q), $\mathbf{P}[s,t]$).
    Place the circulate sub-matrix in the corresponding position within **H**:$\mathbf{H}[(s-1)\times q+1 : s\times M, (t-1)\times M+1 : t\times M]$ = sub-matrix
  end for
end for
Obtain generator matrix of QC-LDPC code.
Consider the parity-check matrix represented as $\mathbf{H} = [\mathbf{A} : \mathbf{B}]$. where **A** is an $M \times M$ matrix & **B** is an $(M \times (N-M))$ matrix.
Construct the generator matrix in systematic form if one of the matrices in **H** is invertible:
$\mathbf{G} = [\mathbf{A}^{-1}\mathbf{B} : \mathbf{I}]$, with $[(N-M)\times M | M\times M]$ dimension.

End Procedure

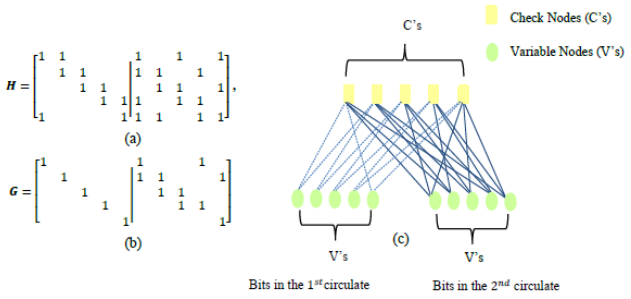

FIGURE 3: An example of QC-LDPC of rate (1⁄2) [29] a. Parity-check matrix with two circulates, b. Generator matrix in systematic form and c. Tanner graph [30].

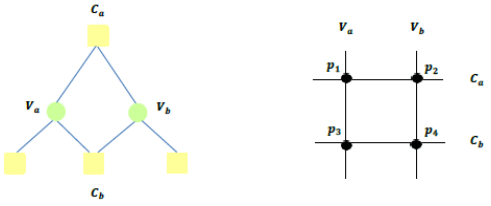

FIGURE 4: An example of a four-cycle a. Tanner graph path, b. Cycle in a parity-check matrix [30]

VIII. QC-LDPC DECODING WITH THE SUM-PRODUCT ALGORITHM

To determine the conditional marginal posterior probabilities $P(\mathbf{x}_{b_i} = 1|\mathbf{xc}_{b_i}; \mathbf{H})$ for individual bits, where $i \in \{1 : N_r\}$. In scenarios where a well-constructed code is employed for communication at an attainable rate, it is typically expected that the posterior probability will strongly focus on the most likely decoding outcome. In our system, the decoding challenge is addressed through utilization of the sum-product algorithm, as detailed in [13] and [31].

This algorithm is particularly relevant for decoding LDPC codes, where the goal is to determine the most likely codeword based on the received noisy signal. Mathematically, the decoding challenge can be formulated as follows:

Let $\mathrm{y}_{b_i n} \in [\mathrm{y}_{b_i 1} : \mathrm{y}_{b_i N}]$ denote the received signal vector of length N from the channel. The objective is to identify the most likely transmitted codeword $\mathbf{xc}_{b_i} = [\mathrm{xc}_{b_i 1} : \mathrm{xc}_{b_i N}]$ that fulfills the requirements of the parity-check equations specified by the parity check matrix $\mathbf{H}$. The decoding problem aims to identify the most likely vector $\mathbf{x}_{b_i}$ such that $\mathbf{H}.\hat{\mathbf{x}}_{b_i} = 0$, where the likelihood of $\mathbf{xc}_{b_i}$ is determined by $\prod_n f_n^{\mathrm{xc}_{b_i n}}$. where $f_n{}^1 = 1/(1 + \exp\left(-2a\mathrm{y}_{b_i n}/\sigma^2\right))$ and $f_n^0 = 1 - f_n^1$, and $\mathrm{y}_{b_i n}$ denotes the channel output at time n. During each iteration, a probability ratio is transmitted along every edge within the graph, and every bit node $\mathrm{xc}_{b_i n}$. Update its probability of being in State 1. The set of bits indexed by n associated with check m as $N(m) = \{n : \mathbf{H}_{mn} = 1\}$. Similarly, the checks for which bit n is involved as $M(n) = \{m : \mathbf{H}_{mn} = 1\}$. The term $q_{mn}^{\mathrm{xc}_{b_i n}}$ denotes the probability that the n^{th} bit of $\mathbf{xc}_{b_i}$ has the value $\mathrm{xc}_{b_i n}$, considering the information gathered from checks other than check m. The term $r_{mn}^{\mathrm{xc}_{b_i n}}$ denotes the probability of check m being satisfied when bit n of $\mathbf{xc}_{b_i}$ remains constant at $\mathrm{xc}_{b_i n}$, while the other bits have distinct distributions determined by the probabilities $\{q_{mn'} : n' \in N(m)\backslash n\}$. The algorithm generates precise posterior probabilities for all bits after a specified number of iterations, provided that the bipartite graph described by the matrix $\mathbf{H}$ is cycle-free.

- **Initialization:** Let $f_n^0 = P(\mathrm{xc}_{b_i n} = 0)$ represent the prior probability of bit x_{b_i} being 0, and $f_n^1 = P(\mathrm{xc}_{b_i n} = 1) = 1 - f_n^0$. In the context of syndrome decoding, when the channel operates as a binary symmetric channel, f_n^1 becomes equal to f. If the noise level follows a known pattern, f_n^1 is adjusted to the corresponding normalized likelihood. For every (n, m) where $\mathbf{H}_{mn} = 1$, the values of the variables q_{mn}^0 and q_{mn}^1 are set to f_n^0 and f_n^1 respectively.
- **Horizontal Step:** We define $\delta_{q_{mn}} = q_{mn}^0 - q_{mn}^1$ and compute for each m, n:

$$\delta_{r_{mn}} = \prod_{n' \in N(m)\backslash\{n\}} \delta_{qmn'} \tag{28}$$

  Then, set $r_{mn}^0 = \frac{1}{2}(1 + \delta_{r_{mn}})$ and $r_{mn}^1 = \frac{1}{2}(1 - \delta_{r_{mn}})$.
- **Vertical Step:** For each n and m and for $\mathrm{xc}_{b_i n} = 0, 1$ we update:

$$q_{mn}^{\mathrm{xc}_{b_i n}} = \alpha_{mn} f_n^{\mathrm{xc}_{b_i n}} \prod_{m_0' \in M(n)\backslash\{m\}} r_{m'n}^0 \tag{29}$$

  where α_{mn} is selected such that $q_{mn}^0 + q_{mn}^1 = 1$. We can also update the 'pseudo-posterior probabilities as:

$$q_{mn}^{\mathrm{xc}_{b_i n}} = \alpha_n f_n^{\mathrm{xc}_{b_i n}} \prod_{m \in M(n)} r_{mn}^{\mathrm{xc}_{b_i n}}.$$

  These quantities are employed to generate a preliminary bit-by-bit decoding $\hat{\mathrm{x}}_{b_i n}$; if $\mathbf{H}.\hat{\mathbf{x}}_{b_i} = 0$ then the decoding process is concluded. Otherwise, the algorithm repeats the horizontal step. A failure is declared if the maximum number of iterations (e.g., 100) occurs without valid decoding.

A. COMPUTATIONAL COMPLEXITY

In the brute-force method, generating the code requires a time complexity of $O(N^3)$, where N denotes the block size. Although the encoding time scales with $O(N^2)$, it is important to highlight that the encoding procedure exclusively uses binary arithmetic. Hence, the encoding time is significantly decreased in comparison with the simulation of the Gaussian channel. The reduction in encoding time can potentially be accomplished by employing sparse matrix techniques. Decoding involves approximately $6Nt$ floating-point multiplications per iteration. Consequently, the total number of operations required per decoded bit (considering 20 iterations) is roughly $120t/R$, irrespective of the block length.

The encoding and decoding methods utilized for QC-LDPC codes, along with the decoding algorithm presented by MacKay and Neal, are well-suited for effective communication with high-speed data rates and minimal error rates. This capability is particularly significant for vehicular communication systems, that require fast and reliable data transmissions.

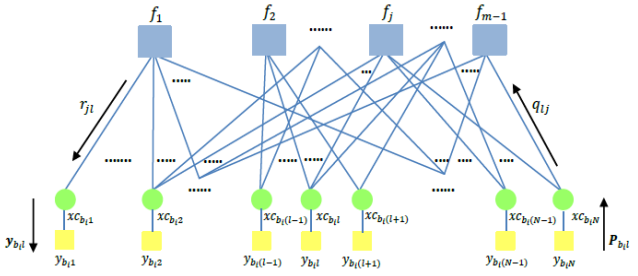

FIGURE 5: A factor graph for decoding LDPC code [32].

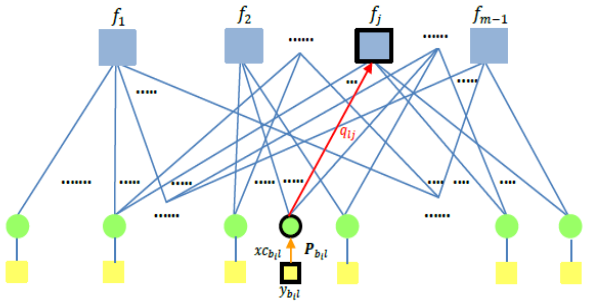

Step 1. Initialize q^{ij}

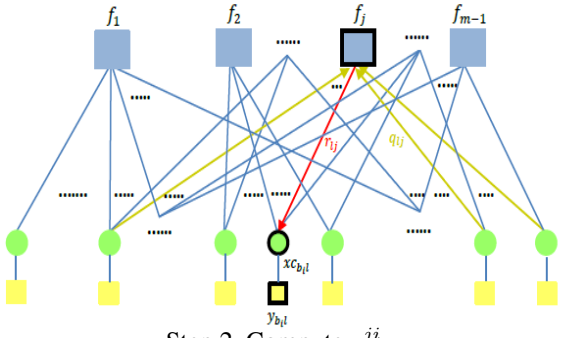

Step 2. Compute r^{ji}

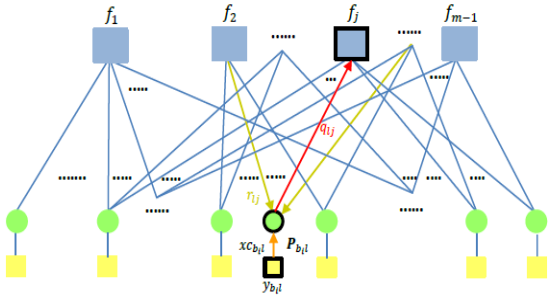

Step 3. Compute q^{ij}

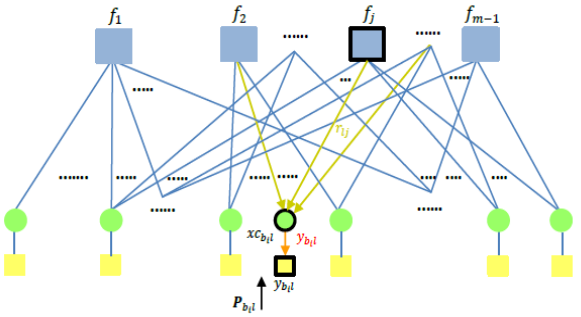

Step 4. y_b^i

IX. BIT ERROR PERFORMANCE ANALYSIS

In this section, we analyze the average pairwise error probability (PEP) for both the ML and SIC detection techniques. We present a precise mathematical expression for the ML approach and an approximate SIC method. In addition, we established an upper limit for the BER using the union bounding technique. As per the union bounding method, the upper bound on the BER of k can be expressed as [33], [34]:

$$\mathrm{BER}_k = \frac{1}{N}\sum_k \tau_k \mathrm{PEP}_k \tag{30}$$

where k is indicated as $(A|B_2)$ and $(A|B_{1\text{-SIC}})$ to represent the line introducing errors at (Bob_2) and (Bob_1) respectively. For these two lines, PEP simply measures the likelihood of erroneously detecting the separated symbol vectors of $(\hat{\mathbf{xc}}_{b_1}, \hat{\mathbf{xc}}_{b_2})$ of length N in the presence of parity bits at (Bob_1) and (Bob_2) respectively, whereas the transmitted vectors for the mentioned detected vectors are represented as $(\mathbf{xc}_{b_1}, \mathbf{xc}_{b_2})$. As illustrated in the System Model section, the detected signal at the near receiver $\hat{\mathbf{xc}}_{b_1}$ is indicated after applying SIC to eliminate the introduced errors from the high-power signal as $\mathbf{xc}_{b_2-\text{detected}}$. ML was then applied to the received clean signal $\mathbf{y}_{b_1-\text{clean}}$. Procedure 1 outlines the steps of the related detector procedure [8]. According to (30), τ_k represents the distance between the detected and transmitted pairs in terms of the number of different bits. For the far user, the average pairwise error probability $\mathrm{PEP}_{A|B_2}$ can be derived as follows:

$$\begin{aligned}\mathrm{PEP}_{A|B_2} = \Pr\Bigg\{ &\left\| \mathbf{y}_{b_2} - P_{d_{(A-B_2)|B_2}}\left(\sum_{i=1}^{N_r} \mathbf{h}_{b_2}(i)\cdot \mathbf{xc}_{b_2}\right)\right\|^2 \\ &> \left\| \mathbf{y}_{b_2} - P_{d_{(A-B_2)|B_2}}\left(\sum_{i=1}^{N_r} \mathbf{h}_{b_2}(i)\cdot \hat{\mathbf{xc}}_{b_2}\right)\right\|^2 \Bigg\}\end{aligned} \tag{31}$$

$$\begin{aligned}&\text{Assuming:} \mathbf{\Lambda}_{A|B_2} \triangleq \sum_{i=1}^{N_r} \mathbf{h}_{b_2}(i)\cdot \mathbf{xc}_{b_2} \quad \& \\ &\hat{\mathbf{\Lambda}}_{A|B_2} \triangleq \sum_{i=1}^{N_r} \mathbf{h}_{b_2}(i)\cdot \hat{\mathbf{xc}}_{b_2}. \\ &\mathrm{PEP}_{A|B_2} = \Pr\Bigg\{ \left\| \mathbf{y}_{b_2} - P_{d_{(A-B_2)|B_2}} \mathbf{\Lambda}_{A|B_2}\right\|^2 \\ &\qquad > \left\| \mathbf{y}_{b_2} - P_{d_{(A-B_2)|B_2}} \hat{\mathbf{\Lambda}}_{A|B_2}\right\|^2 \Bigg\}\end{aligned} \tag{32}$$

Substituting (7) in (32):

$$\text{PEP}_{A|B_2} = \Pr\left\{\|\mathbf{w}_{b_2}\|^2 > \left\|P_{d_{(A-B_2)|B_2}}(\Lambda_{A|B_2} - \hat{\Lambda}_{A|B_2}) + \mathbf{w}_{b_2}\right\|^2\right\} \tag{33}$$

Let, $\boldsymbol{\Delta}_{A|B_2} = \boldsymbol{\Lambda}_{A|B_2} - \hat{\boldsymbol{\Lambda}}_{A|B_2}$.

$$\begin{aligned}\text{PEP}_{A|B_2} &= \Pr\left\{\|\mathbf{w}_{b_2}\|^2 > \left\|P_{d_{(A-B_2)|B_2}}(\boldsymbol{\Delta}_{A|B_2}) + \mathbf{w}_{b_2}\right\|^2\right\} \\ &= \Pr\left(2R(\boldsymbol{\Delta}_{A|B_2}\mathbf{w}^*_{b_2}) > \left\|P_{d_{(A-B_2)|B_2}}(\boldsymbol{\Delta}_{A|B_2})\right\|^2\right)\end{aligned} \tag{34}$$

where $R(\cdot)$ denotes the real part, $(\cdot)^*$ denotes conjugation, and $2R(\boldsymbol{\Delta}_{A|B_2}\mathbf{w}^*_{b_2})$ is a Gaussian random variable with mean zero and variance $2\sigma^2\|\boldsymbol{\Lambda}_{A|B_2}(\boldsymbol{\Delta}_{A|B_2})\|^2$ [34]. Then, the conditional PEP can be expressed using the Q function for a particular channel instance, as follows:

$$\begin{aligned}\text{PEP}_{A|B_2} &= Q\left(\sqrt{\frac{\|P_{d_{(A-B_2)|B_2}}\boldsymbol{\Delta}_{A|B_2}\|^2}{2\sigma^2}}\right) \\ &= Q\left(\sqrt{\frac{\boldsymbol{\Phi}_{A|B_2}}{2\sigma^2}}\right)\end{aligned} \tag{35}$$

where $\boldsymbol{\Phi}_{A|B_2} = \|P_{d_{(A-B_2)|B_2}}(\sum_{i=1}^{N_r}\mathbf{h}_{b_2}(i)\cdot\mathbf{xc}_{b_2} - \sum_{i=1}^{N_r}\mathbf{h}_{b_2}(i)\cdot\hat{\mathbf{x}}\mathbf{c}_{b_2})\|^2 = P_{d_{(A-B_2)|B_2}}\sum_{l=1}^{N}\|\gamma_l\|^2$ and γ_l is the l^{th} element in $\boldsymbol{\Delta}_{A|B_2}$. Given that $\mathbf{h}_{b_2} \sim \mathcal{CN}(0,1)$ and $\boldsymbol{\Phi}_{A|B_2}$ is a sum of N exponential random variables R_{VS} with mean of $\mu_l = P_{d_{(A-B_2)|B_2}}\|\gamma_l\|^2$. On the other hand, the average pairwise error probability at the near receiver is then as follows:

$$\begin{aligned}\text{PEP}_{A|B_1\text{-SIC}} = \Pr\Bigg\{&\left\|\mathbf{y}_{b_1\text{-clean}} - P_{d_{(A-B_1)|B_1}}\left(\sum_{i=1}^{N_r}\mathbf{h}_{b_1}(i)\cdot\mathbf{xc}_{b_1}\right)\right\|^2 \\ &> \left\|\mathbf{y}_{b_1\text{-clean}} - P_{d_{(A-B_1)|B_1}}\left(\sum_{i=1}^{N_r}\mathbf{h}_{b_1}(i)\cdot\hat{\mathbf{x}}\mathbf{c}_{b_1}\right)\right\|^2\Bigg\}\end{aligned} \tag{36}$$

Assuming: $\boldsymbol{\Lambda}_{A|B_1\text{-SIC}} \triangleq \sum_{i=1}^{N_r}\mathbf{h}_{b_1}(i)\cdot\mathbf{xc}_{b_1}$ & $\hat{\boldsymbol{\Lambda}}_{A|B_1\text{-SIC}} \triangleq \sum_{i=1}^{N_r}\mathbf{h}_{b_1}(i)\cdot\hat{\mathbf{x}}\mathbf{c}_{b_1}$.

$$\begin{aligned}\text{PEP}_{A|B_1\text{-SIC}} = \Pr\Bigg\{&\left\|\mathbf{y}_{b_1\text{-clean}} - P_{d_{(A-B_1)|B_1}}\boldsymbol{\Lambda}_{A|B_1\text{-SIC}}\right\|^2 \\ &> \left\|\mathbf{y}_{b_1\text{-clean}} - P_{d_{(A-B_1)|B_1}}\hat{\boldsymbol{\Lambda}}_{A|B_1\text{-SIC}}\right\|^2\Bigg\}\end{aligned} \tag{37}$$

Substituting the equation of $\mathbf{y}_{b_1\text{-clean}}$ from Procedure (1) in (37):

$$\begin{aligned}\text{PEP}_{A|B_1\text{-SIC}} = \Pr\Bigg\{&\|\mathbf{w}_{b_1}\|^2 \\ &> \left\|P_{d_{(A-B_1)|B_1}}(\boldsymbol{\Lambda}_{A|B_1\text{-SIC}} - \hat{\boldsymbol{\Lambda}}_{A|B_1\text{-SIC}}) + \mathbf{w}_{b_1}\right\|^2\Bigg\}\end{aligned} \tag{38}$$

Let, $\boldsymbol{\Delta}_{A|B_1\text{-SIC}} = \boldsymbol{\Lambda}_{A|B_1\text{-SIC}} - \hat{\boldsymbol{\Lambda}}_{A|B_1\text{-SIC}}$.

$$\begin{aligned}\text{PEP}_{A|B_1\text{-SIC}} = \Pr\Bigg\{&\|\mathbf{w}_{b_1}\|^2 \\ &> \left\|P_{d_{(A-B_1)|B_1}}(\boldsymbol{\Delta}_{A|B_1\text{-SIC}}) + \mathbf{w}_{b_1}\right\|^2\Bigg\} \\ &= \Pr\left(2R(\boldsymbol{\Delta}_{A|B_1\text{-SIC}}\mathbf{w}^*_{b_1}) > \left\|P_{d_{(A-B_1)|B_1}}(\boldsymbol{\Delta}_{A|B_1\text{-SIC}})\right\|^2\right)\end{aligned} \tag{39}$$

where $R(\cdot)$ denotes the real part, $(\cdot)^*$ denotes conjugation, and $2R(\boldsymbol{\Delta}_{A|B_1\text{-SIC}}\mathbf{w}^*_{b_1})$ is a Gaussian random variable with mean zero [34] and variance $2\sigma^2\left\|\Lambda_{A|B_1\text{-SIC}}(\boldsymbol{\Delta}_{A|B_1\text{-SIC}})\right\|^2$. Therefore,

$$\begin{aligned}\text{PEP}_{A|B_1\text{-SIC}} &= Q\left(\sqrt{\frac{\|P_{d_{(A-B_1)|B_1}}\boldsymbol{\Delta}_{A|B_1\text{-SIC}}\|^2}{2\sigma^2}}\right) \\ &= Q\left(\sqrt{\frac{\boldsymbol{\Phi}_{A|B_1\text{-SIC}}}{2\sigma^2}}\right)\end{aligned} \tag{40}$$

As it was obtained in (40), it can be possible to represent $\boldsymbol{\Phi}_{A|B_1\text{-SIC}}$ as: $|P_{d_{A-B_1|B_1}}(\sum_{i=1}^{N_r}\mathbf{h}_{b_1}(i)\cdot\mathbf{xc}_{b_1} - \sum_{i=1}^{N_r}\mathbf{h}_{b_1}(i)\cdot\hat{\mathbf{x}}\mathbf{c}_{b_1})|^2 = P_{d_{A-B_1|B_1}}\sum_{l=1}^{N}\|\gamma_l\|^2$, where γ_l is the l^{th} element in $\boldsymbol{\Delta}_{A|B_1\text{-SIC}}$. There are $K \leq MR_{VS}$ with nonzero means. Furthermore, R out of KR_{VS} has a unique means $[\mu_1 : \mu_R]$, as considered in formula (12) in [34].

According to a previous study, there is $K \leq NR_{VS}$ has a nonzero mean. Furthermore, there are R out of KR_{VS} has a unique mean $[\mu_1 : \mu_R]$. Let us denote the number of R_{VS} with mean μ_i as r_i. Therefore, the PDF of $\boldsymbol{\Phi}_{i,k}$ is given in [33], as follows:

$$f_{\boldsymbol{\Phi}_{i,k}}(\theta) = \sum_{q=1}^{R}\lambda_q^{r_q}e^{-\theta\lambda_q}\sum_{w=1}^{r_q}A_{q,w}\frac{(-1)^{r_q-w}}{(w-1)!}\theta^{w-1} \tag{41}$$

where,

$$A_{q,w} = \sum_{\substack{m_1+\cdots+m_R\\=r_q-w\\m_q=0}}\prod_{\substack{t=1\\t\neq q}}^{R}\left(\binom{r_t+m_t-1}{m_t}\frac{\lambda_t^{r_t}}{(\lambda_t-\lambda_q)^{r_t+m_t}}\right) \tag{42}$$

and $\lambda_l = \frac{1}{\mu_l}$

After integrating equations (35) and (40) across the probability density function outlined in (41) and employing a

methodology similar to that in [34], followed the same steps as in [35] with more details in [36] , we derive:

$$\begin{aligned}\text{PEP} = &\sum_{q=1}^{R} \lambda_q^{r_q} \sum_{w=1}^{r_q} A_{q,w}(-1)^{r_q-w} \left(\frac{\chi_q}{\lambda_q}\right) \\ &\times \sum_{p=0}^{w-1} \binom{w-1+p}{p} (1-\chi_q)^p\end{aligned} \tag{43}$$

where $\chi_q = \frac{1}{2}\left(1 - \frac{1}{\sqrt{1+4\sigma^2\lambda_q}}\right)$ and the BER for each transmission line $(A|B_2)$ and $(A|B_{1\text{-SIC}})$ can be obtained by substituting (43) in to (30) individually.

X. SINR AND SUM RATE ANALYSIS

In this section, we evaluate the sum rate of each user in the proposed system as it was calculated in [37], [38], [39] and [40]. As, (Bob_2) does not need to perform SIC because it comes first in decoding order. Therefore, (Bob_2) decodes its received signal $\mathbf{xc}_{b_2}$ by directly treating $\mathbf{xc}_{b_1}$ as an interference. So, for (Bob_2) the SINR is given as:

$$\gamma_{Bob_2} = \frac{P_t \cdot \alpha_{b_2} \cdot d_{(A-B_2)}^{-\eta} \cdot |\mathbf{h}_{b_2}|^2}{P_t \cdot \alpha_{b_1} \cdot d_{(A-B_2)}^{-\eta} \cdot |\mathbf{h}_{b_2}|^2 + \sigma^2} \tag{44}$$

The achievable data rate expression for (Bob_2) can be represented in terms of γ_{Bob_2} as:

$$R_{\text{Bob}_2} = \log_2(1 + \gamma_{\text{Bob}_2}) \tag{45}$$

By substituting (44) into (45), R_{Bob_2} can be written as:

$$\begin{aligned}R_{\text{Bob}_2} &= \log_2\left(1 + \frac{P_t \cdot \alpha_{b_2} \cdot d_{A-B_2}^{-\eta} \cdot |\mathbf{h}_{b_2}|^2}{P_t \cdot \alpha_{b_1} \cdot d_{A-B_2}^{-\eta} \cdot |\mathbf{h}_{b_2}|^2 + \sigma^2}\right) \\ &= \log_2\left(1 + \frac{P_{d_{(A-B_2)|B_2}}^2 \cdot |\mathbf{h}_{b_2}|^2}{P_{d_{(A-B_2)|B_1}}^2 \cdot |\mathbf{h}_{b_2}|^2 + \sigma^2}\right)\end{aligned} \tag{46}$$

Unlike (Bob_2), (Bob_1) initially detects $\mathbf{xc}_{b_2}$ to subtract its component from the received signal $\mathbf{y}_{b_1}$. The SINR expression at (Bob_2) for decrypting the (Bob_1) signal before SIC is given by:

$$\gamma_{\text{Bob}_2 \to \text{Bob}_1} = \frac{P_t \cdot \alpha_{b_1} \cdot d_{A-B_1}^{-\eta} \cdot |\mathbf{h}_{b_1}|^2}{P_t \cdot \alpha_{b_2} \cdot d_{A-B_1}^{-\eta} \cdot |\mathbf{h}_{b_1}|^2 + \sigma^2} \tag{47}$$

The achievable data rate at (Bob_1) can then be represented as:

$$\begin{aligned}R_{\text{Bob}_2 \to \text{Bob}_1} &= \log_2\left(1 + \gamma_{\text{Bob}_2 \to \text{Bob}_1}\right) \\ &= \log_2\left(1 + \frac{P_t \cdot \alpha_{b_1} \cdot d_{A-B_1}^{-\eta} \cdot |\mathbf{h}_{b_1}|^2}{P_t \cdot \alpha_{b_2} \cdot d_{A-B_1}^{-\eta} \cdot |\mathbf{h}_{b_1}|^2 + \sigma^2}\right) \\ &= \log_2\left(1 + \frac{P_{d_{(A-B_1)|B_1}}^2 \cdot |\mathbf{h}_{b_1}|^2}{P_{d_{(A-B_1)|B_2}}^2 \cdot |\mathbf{h}_{b_1}|^2 + \sigma^2}\right)\end{aligned} \tag{48}$$

As $R_{\text{Bob}_2 \to \text{Bob}_1} > R_{\text{Bob}_2}$ is ensured, which means $\mathbf{xc}_{b_2}$ can be eliminated entirely with the assistance of SIC at (Bob_1). After subtracting $\mathbf{xc}_{b_2}$ from $\mathbf{y}_{b_1}$, the achievable data rate of (Bob_1) decoding its own signal $\mathbf{xc}_{b_1}$ is expressed as:

$$R_{\text{Bob}_1} = \log_2\left(1 + \frac{P_{d_{(A-B_1|B_1)}}^2 \cdot |\mathbf{h}_{b_1}|^2}{\sigma^2}\right) \tag{49}$$

When considering the increment in the numbers of transmitted and received antennas, the user with a bad channel condition is assigned a higher transmission power than others with good channel conditions. Consequently, the user with the highest transmission power treats signals from other users as noise; it promptly recovers its signal and the achievable data rate can be calculated as in (49). Therefore, the SINR for the remaining users γ_{Bob_z} in our proposed system after the aforementioned expansion can be calculated by considering $l = [0 : N_r - 2]$ and $z = N_r - l$:

$$\gamma_{\text{Bob}_z} = \frac{P_t \cdot \alpha_{b_z} \cdot d_{A-B_z}^{-\eta} \cdot |\mathbf{h}_{b_z}|^2}{P_t \cdot \sum_{j=1}^{z-1} \alpha_{b_j} \cdot d_{A-B_z}^{-\eta} \cdot |\mathbf{h}_{b_z}|^2 + \sigma^2} \tag{50}$$

After obtaining the SINR expressions of downlink NOMA, the sum rate can be easily analyzed. The achievable data rate of the z^{th} user (Bob_z) in the downlink NOMA-MIMO/QC-LDPC system can be expressed as:

$$R_{\text{Bob}_z} = \log_2\left(1 + \frac{P_{d_{(A-B_z)|B_z}}^2 \cdot |\mathbf{h}_{b_z}|^2}{P_t \cdot \sum_{j=1}^{z-1} \alpha_{b_j} \cdot d_{A-B_z}^{-\eta} \cdot |\mathbf{h}_{b_z}|^2 + \sigma^2}\right) \tag{51}$$

Then, the sum rate of the proposed can be written as:

$$\begin{aligned}R_{\text{Bob}_z}^{\text{MIMO-NOMA}} = &\sum_{l=0}^{N_r-2} \log_2\left(1 + \frac{P_{d_{(A-B_z)|B_z}}^2 \cdot |\mathbf{h}_{b_z}|^2}{P_t \sum_{j=1}^{z-1} \alpha_{b_j} \cdot d_{A-B_z}^{-\eta} \cdot |\mathbf{h}_{b_z}|^2 + \sigma^2}\right) \\ &+ \log_2\left(1 + \frac{P_{d_{(A-B_1)|B_1}}^2 \cdot |\mathbf{h}_{b_1}|^2}{\sigma^2}\right)\end{aligned} \tag{52}$$

XI. THE OUTAGE PROBABILITY ANALYSIS OF THE PROPOSED SYSTEM OVER RICIAN FADING CHANNEL

Analyzing the outage probability is crucial for determining the robustness and reliability of NOMA-MIMO systems, particularly in challenging scenarios such as (V2V) communications, where channel conditions are often highly dynamic and unpredictable. Outage probability refers to the probability that a user's signal cannot be decoded successfully owing to inadequate signal quality, which occurs when the communication link fails to meet a specific (QoS) standard. This typically happens when the SNR drops below a predefined threshold.

By enabling simultaneous transmission, NOMA enhances the efficient use of available resources, which can lead to a reduction in the overall outage probability of the system. It utilizes the diversity in channel conditions among users, allowing those with varying levels of channel quality to share the same resources, thereby improving overall system performance. The diversity introduced by multiple users

transmitting simultaneously helps mitigate the fading effects and boosts the reliability of the communication link, ultimately reducing the outage probability. Meanwhile, the QC-LDPC codes without $Girth_4$ cycles offer greater resilience to error propagation, particularly in high-noise environments. Avoiding $Girth_4$ cycles prevents the poor performance that can occur in certain scenarios, thereby enhancing the overall effectiveness of the codes. This improves the decoder's ability to correct errors, which in turn lowers the probability of decoding failures and boosts overall system reliability. The improved error-correcting capabilities result in a decreased error rate, leading to a lower probability of the SNR dropping below the required threshold. Consequently, this directly reduces the outage probability of the communication system, ensuring a stable communication link even at high vehicular speeds.

This section presents a closed-form expression for the outage probability over the Rician fading channel for Bob2 and Bob_1, as derived from [41].

For Bob_2:

Based on (46), the outage condition for a user in a Rician fading channel is expressed as:

$$R_{\text{Bob}_2} < R^T_{\text{Bob}_2} \tag{53}$$

Assuming $|\mathbf{h}_{b_2}|^2 = \gamma_2$.The simplified form of (53) can be written as:

$$\gamma_2 < \frac{\sigma^2 \cdot R^T_{\text{Bob}_2}}{P^2_{d(A-B_2)|B_2} - P^2_{d(A-B_2)|B_1} \cdot R^T_{\text{Bob}_2}} \tag{54}$$

The PDF of the Rician fading channel [41], [42] is given by:

$$P_\gamma(\gamma) = \frac{1+K}{\bar{\gamma}} e^{-K-\frac{(1+K)\gamma}{\bar{\gamma}}} I_0\left(2\sqrt{\frac{K(1+K)\gamma}{\bar{\gamma}}}\right), \gamma \geq 0 \tag{55}$$

The channel gain follows an exponential distribution and is related to the first-order modified Bessel function in its mathematical description.

To obtain the closed-form expression, we integrate (55) with respect to γ after applying the following simplifications.:

$$\mathcal{E}_{\text{Bob}_2} = \frac{\sigma^2 \cdot R^T_{\text{Bob}_2}}{P^2_{d(A-B_2)|B_2} - P^2_{d(A-B_2)|B_1} \cdot R^T_{\text{Bob}_2}} \tag{56}$$

$$P_{\text{outage2}} = \int_0^{\mathcal{E}_{\text{Bob}_2}} \frac{(1+K)}{\bar{\gamma}} e^{-K-\frac{(1+K)\gamma}{\bar{\gamma}}} \times I_0\left(2\sqrt{\frac{K(1+K)\gamma}{\bar{\gamma}}}\right) \gamma \, d\gamma \tag{57}$$

Replacing $\frac{K(1+K)\gamma}{\bar{\gamma}} = \psi^2$, it can be able to get:

$$P_{\text{outage2}} = 1 - \frac{(1+K)}{\bar{\gamma}} e^{-K} \times \int_{\max\left(\sqrt{\frac{1+K}{\bar{\gamma}}}, \mathcal{E}_{\text{Bob}_2}\right)}^{\infty} e^{-\psi^2} I_0\left(2\sqrt{K\psi^2}\right) \frac{2\psi\bar{\gamma}}{1+K} \, d\psi \tag{58}$$

Following further simplification, the closed-form expression for the outage probability of a distant user over a Rician fading channel is obtained as follows:

$$P_{\text{outage2}} = 1 - Y_{\frac{1}{2}}\left(2\sqrt{K}, \sqrt{\frac{1+K}{\bar{\gamma}}}, \mathcal{E}_{\text{Bob}_2}\right) \tag{59}$$

where $Y_\delta(\alpha, \beta)$ is defined as in [41], [43]

$$Y_\delta(\alpha,\beta) = \frac{\sqrt{\pi}(1-\alpha^2)2^{\left(\frac{2}{3}\right)-\delta}}{\Gamma(s)H^{(\delta-0.5)}\alpha^{(-\delta+0.5)}} \times \int_\beta^\infty \mathcal{E}^{2\mu} e^{-\mathcal{E}^2} I_{(\delta-0.5)}(\alpha^2\mathcal{E}) \, d\mathcal{E} \tag{60}$$

For Bob_1:

Based on (49), the outage condition for a user in a Rician fading channel is expressed as:

$$R_{\text{Bob}_1} < R^T_{\text{Bob}_1} \tag{61}$$

we assumed that $|\mathbf{h}_{b_1}|^2 = \gamma_1$ and $\mathcal{E}_{\text{Bob}_1} = \frac{\sigma^2 \cdot R^T_{\text{Bob}_1}}{P^2_{d(A-B_1)|B_1}}$.The simplified form of (61) can be written as:

$$\gamma_1 < \max\{\mathcal{E}_{\text{Bob}_2}, \mathcal{E}_{\text{Bob}_1}\} \tag{62}$$

After additional simplification, the closed-form expression for the outage probability of a nearby user over a Rician fading channel is derived as:

$$P_{\text{outage1}} = 1 - Y_{1/2}\left(2\sqrt{K}, \sqrt{\frac{1+K}{\bar{\gamma}}}, \max\{\mathcal{E}_{\text{Bob}_2}, \mathcal{E}_{\text{Bob}_1}\}\right) \tag{63}$$

In such communication environments, high mobility results in frequent handovers and fluctuating channel conditions, which can increase the risk of outages. The Rician fading model incorporates both LOS and multi-path components, which are typical in vehicular settings. The fading characteristics of such channels can considerably affect the performance of the communication systems. The QC-LDPC codes can help alleviate the impact of fading by enhancing the reliability of the transmitted data.

XII. QUANTIFYING THE IMPACT OF QC-LDPC ON THE SYSTEM PERFORMANCE

Utilizing QC-LDPC codes without $Girth_4$ cycles can result in improvements not only in terms of BER but also in the sum rates for nearby and distant users. The improvement achieved depends on the MIMO configuration and coding rate of the QC-LDPC code. The optimal QC-LDPC code rate for error correction depends on several variables, including the properties of the communication channel, the extent of noise and interference, and the specific requirements of the application. When a communication system operates close to the Shannon limit, it indicates that the system is making optimal use of the channel resources, transmitting information at the highest feasible rate while still ensuring reliability. This indicates that

the system effectively mitigated the effects of channel noise and interference.

Mathematically, the rate of QC-LDPC codes without $Girth_4$, denoted previously by $(R \geq 1 - k/j)$, can enhance the performance of the NOMA system in terms of error correction and sum rate. The BER of the NOMA technique in our proposed system depends on PEP_k for both ML and SIC detection techniques which are analyzed and calculated for both (Bob_2) and (Bob_1) as in (35) and (40) respectively. The error correction capability of QC-LDPC codes is characterized by their ability to reduce PEP_k for the calculated SINRs, as shown in (50). Accordingly, the sum rate of the proposed downlink NOMA-MIMO/QC-LDPC system is then evaluated as in (50). QC-LDPC codes without $Girth_4$ are inherently flexible and can be designed to accommodate different code rates without requiring substantial alterations to the code structure. This adaptability enables the QC-LDPC to address a wide range of communication scenarios and effectively meet diverse requirements. Moreover, the design flexibility of the QC-LDPC permits the development of codes that achieve a balance between error correction capability and data rate efficiency, particularly at lower rates.

Vehicular communication systems often operate in real-time and require low-latency processing. The probabilistic decoding algorithm offers computational advantages in terms of message-passing efficiency, particularly in large graphical models. The Mackay96 decoding structure is a specific algorithm designed for QC-LDPC codes, offering improved decoding accuracy, faster convergence, and better error correction capabilities compared to Gallager decoding. This decoding structure supports soft-decision decoding, in which the decoder considers the reliability of the received symbols rather than treating them as binary values. The iterative nature of the Mackay96 decoding structure allows adaptation to varying channel conditions. By iteratively updating the likelihood information of the received symbols, the decoder can adjust its decoding decisions based on the changing channel quality, leading to improved performance in terms of the capacity and BER in NOMA systems.

XIII. RESULTS AND DISCUSSIONS

In this section, the simulated results are provided to evaluate the performance of the proposed NOMA-MIMO/QC-LDPC scheme. The system parameters were set as follows: the path loss exponent was $\eta = 4$, and the distances for the transmission links were assumed to be $d_{A-B_2} = 1000$ m and $d_{A-B_1} = 500$ m. The power allocation factors are set at $\alpha_{b_2} = 0.75$ for (Bob_2) and $\alpha_{b_1} = 0.25$ for (Bob_1). For the QC-LDPC code, it is assumed that the prime number of ranks (q) of the sub-matrices is equal to 87 [30], and the maximum number of iterations is set to 20 $(Iter_{max} = 20)$.

A. BIT ERROR RATE RESULTS

The BER performance of the proposed system is compared with other techniques, namely NOMA-SM [8] and OFDM-LDPC [16], which serve as references for our proposed vehicular communication system based on QC-LDPC. This study focuses on the impact of the antenna configurations and BER performance. This highlights the knowledge gained through comparison and its influence on the design and enhancement of V2V communication systems. The encoding method of SM involves dynamically changing the index of the active Transmit Antenna (TA) symbol-by-symbol, necessitating rapid (Radio Frequency) RF switching. Moreover, achieving a suitable BER performance with SM necessitates a low correlation among the spatial stream channels. Therefore, when designing TA arrays for SM systems, careful consideration of the channel correlation and mutual coupling effects is crucial to achieve suitable BER performance. Consequently, the dynamic nature of vehicular system channels over time leads to a decline in BER performance. According to [16], the LDPC employs longer blocks in its parity-check matrix, leading to fewer signal errors compared to the convolution codes. This requires minimal hardware alterations, which will become crucial as the number of vehicles steadily increases. The previously mentioned systems were compared based on the number of transmitted and received antennas, considering cases where both $N_t = N_r = 2$ and $N_t = N_r = 4$. The results are shown in Figs.6 and 7 respectively.

1) (2×2) MIMO Configuration

For these reasons, as observed in Fig.6, the proposed system outperforms both references, while the vehicular communication system [16] delivers superior performance compared to [8]. Furthermore, according to the NOMA principle, where the SIC is perfectly applied to (Bob_1) exhibits better performance than (Bob_2). Given that the channel gain of (Bob_1) surpasses that of (Bob_2).

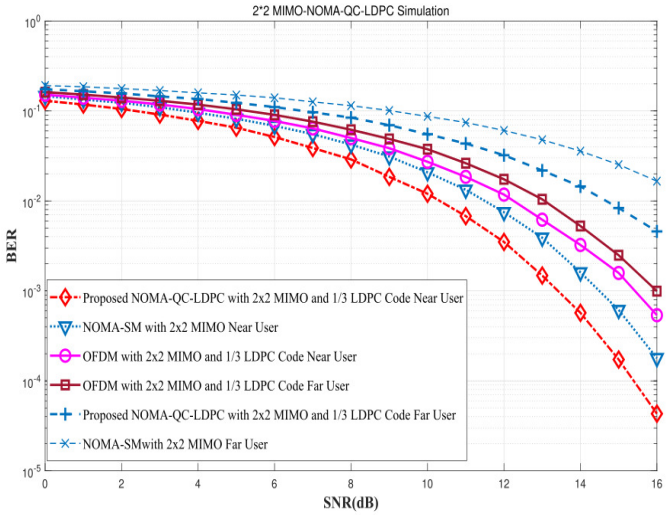

FIGURE 6: BER Comparison for (2×2) MIMO among NOMA-SM, OFDM-(1⁄3) LDPC Code and proposed NOMA-MIMO/QC-LDPC with (1⁄3) LDPC Code for Far User (Bob_2) and Near User (Bob_1) respectively.

2) (4×4) MIMO Configuration

With an increasing number of antennas, the two references are also examined depending on the previous consideration, and the obtained results are illustrated in Fig. 7. This demonstrates further enhancement in our proposed system when $N_t = N_r = 4$ compared to the outcomes when $N_t = N_r = 2$. Increasing the number of antennas introduces diversity to the system, leveraging variations among the channels or paths experienced by each antenna, leading to lower error probabilities.

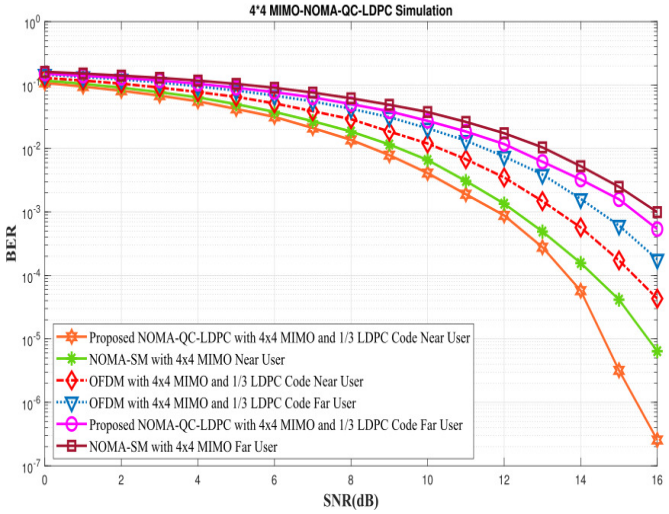

FIGURE 7: BER Comparison for (4×4) MIMO among NOMA-SM, OFDM-(1⁄3) LDPC Code and proposed NOMA-MIMO/QC-LDPC with (1⁄3) LDPC Code for Far User (Bob_2) and Near User (Bob_1) respectively.

B. ACHIEVABLE CAPACITY RESULTS

1) (2×2) MIMO Configuration

Fig.8 illustrates the achievable capacity for a 2×2 MIMO configuration across different communication schemes, focusing on the performance of NOMA integrated with QC-LDPC coding without $Girth_4$. The results indicate that the proposed NOMA-MIMO/QC-LDPC system outperforms both NOMA-SM and OFDM systems, particularly in terms of achievable rates for the near user (Bob_1), which benefits from better channel conditions than the farther one, leading to superior performance. Additionally, the capacity results are plotted as a function of varying transmit power levels, showing that all systems exhibit improvements with increased power. However, the NOMA-MIMO/QC-LDPC system consistently achieved higher rates than other alternatives. These findings highlight that the proposed system effectively uses the available transmit power and leverages the diversity of the MIMO setup, resulting in reduced error probabilities and enhanced capacity. NOMA aims to serve multiple users simultaneously by allocating power according to the channel conditions. However, this approach can lead to performance degradation for users with poor channel conditions. By contrast, OFDM provides a more uniform performance across users, particularly in scenarios where the channel conditions do not differ significantly. For the far user (Bob_2), the OFDM-based vehicular system outperformed NOMA-SM. This is because the NOMA power allocation strategy, which prioritizes users with better channel conditions, can negatively affect those with poorer conditions. Conversely, OFDM ensures more consistent performance across users when the channel conditions are relatively uniform. The capacity results were plotted against varying transmit power levels. As the transmit power increases, the achievable rates for all systems improve; however, the proposed NOMA-MIMO/QC-LDPC system consistently exhibits higher rates than the alternatives. The results demonstrate that the proposed system effectively utilizes the available transmit power and the diversity introduced by the MIMO setup leads to lower error probabilities, thereby enhancing the achievable capacity.

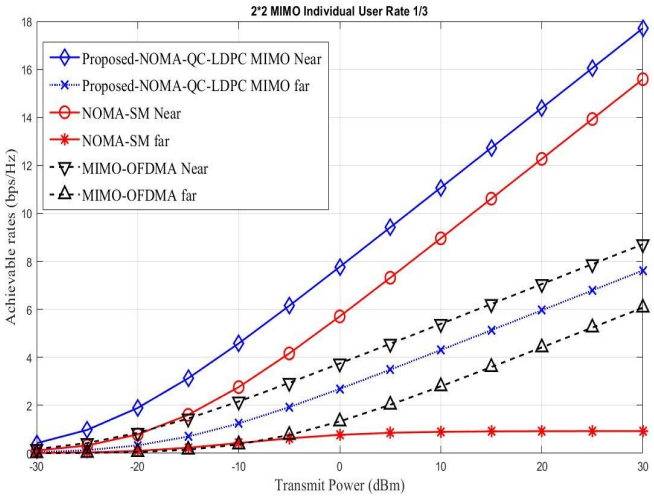

FIGURE 8: Capacity Comparison for (2×2) MIMO among NOMA-SM, OFDM-(1⁄3) LDPC Code and proposed NOMA-MIMO/QC-LDPC with (1⁄3) LDPC Code for Far User (Bob_2) and Near User (Bob_1) respectively.

2) (4×4) MIMO Configuration

Fig.9 compares the capacity of a (4×4) MIMO configuration across different communication schemes, as shown in Fig.8, illustrating how achievable rates (in bps/Hz) vary with transmit power levels (in dBm) for both near and far users. As the transmit power increases, the achievable capacity generally improves across all schemes, emphasizing the benefits of higher power in enhancing signal quality and throughput. Among the evaluated schemes, the proposed NOMA-MIMO/QC-LDPC scheme consistently showed superior performance compared to both NOMA-SM and OFDM with LDPC coding across all transmit power levels, demonstrating that combining NOMA with QC-LDPC coding significantly enhances the system capacity (4×4) MIMO setup. For the

near user, OFDM with (1/3) LDPC coding exhibited the lowest achievable capacity among the three schemes. This could be due to its limitations in adapting to dynamic channel conditions and interference in vehicular environments, as well as the lack of additional advantages offered by NOMA. A (4×4) MIMO system, with a higher number of antennas, offers increased diversity that helps reduce the impact of fading and interference. This enhanced diversity results in a lower BER and more reliable communication, thereby improving the effective capacity of the system compared to a (2×2) configuration. This makes (4×4) MIMO systems better suited for high-capacity applications, such as vehicular communications, where both high data rates and reliability are essential.

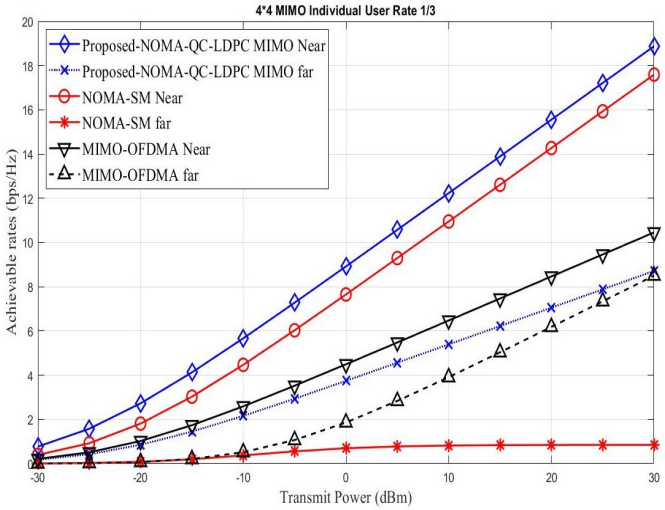

FIGURE 9: Capacity Comparison for (4×4) MIMO among NOMA-SM, OFDM-(1⁄3) LDPC Code and proposed NOMA-MIMO/QC-LDPC with (1⁄3) LDPC Code for Far User (Bob_2) and Near User (Bob_1) respectively.

C. OUTAGE PROBABILITY RESULTS

Figure 10 illustrates the outage probability for various communication schemes, including the proposed NOMA-MIMO/QC-LDPC system, NOMA-SM, and OFDM with (1/3) LDPC coding, across different transmit power levels (in dBm). The results show that as the transmit power increases, the outage probability decreases for all users, which is particularly beneficial for far user (Bob_2) who generally suffers from higher outage rates due to poorer channel conditions. The NOMA-MIMO/QC-LDPC system demonstrates its effectiveness in enhancing the reliability of V2V communication by integrating NOMA's resource allocation strategy with the error-correcting capabilities of QC-LDPC codes without $Girth_4$, resulting in a significant reduction in outage probability, especially in challenging vehicular environments. Although OFDM offers a more uniform performance across users, it does not match the reliability achieved by the NOMA-MIMO/QC-LDPC system, particularly for users experiencing poorer channel conditions. The power allocation strategy in NOMA tends to prioritize the near user (Bob_1), which can cause the far user (Bob_2) to experience higher error rates due to the weaker signal strength and increased susceptibility to noise and interference. However, the robust error correction capabilities of the QC-LDPC help sustain strong performance even under weaker signal conditions, making it more suitable for users located further away. Meanwhile, the (Bob_2) benefits from improved channel conditions, higher power allocation, and the advantages of spatial modulation, leading to better performance and reduced error rates. These findings are particularly crucial for applications like (V2V) communications, where reliable performance is essential in dynamic environments.

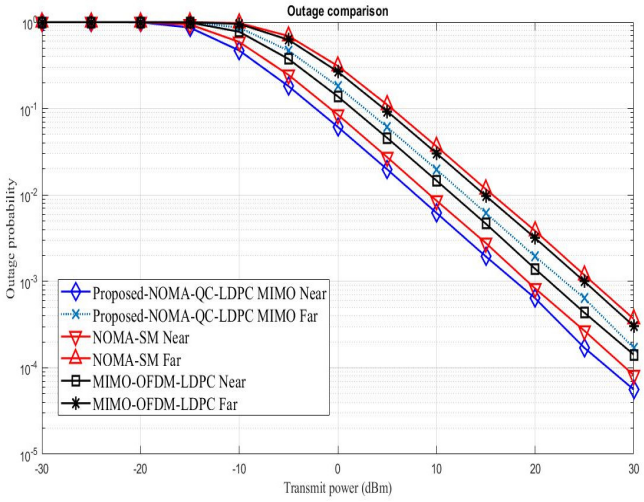

FIGURE 10: The outage performance of (Bob_1) and (Bob_2) in the proposed NOMA-MIMO/QC-LDPC system versus transmit power (dBm) in comparision with NOMA-SM, OFDM-(1⁄3) LDPC Code systems over Rician fading channel.

D. RESULTS UNDER THE INFLUENCE OF DOPPLER EFFECT

The Doppler shift affects vehicular communication systems by altering the received signal frequency owing to the relative motion between the transmitter and receiver, where signals travel along multiple paths with varying lengths and velocities. The corresponding frequency shift can cause the received signal to differ from the intended frequency, thereby leading to challenges in demodulation and decoding. Such distortions can increase the BER, causing the receiver to misinterpret transmitted bits. As the BER increases owing to Doppler shifts, the effective throughput of the communication system decreases, with higher error rates necessitating retransmissions and reducing the overall data rate. Numerous studies have examined V2V communication using MIMO technology, particularly focusing on the impact of Doppler shifts on system performance. The most relevant studies were as follows:

1) MIMO System based on NOMA-SM

The system in [8] considered a maximum Doppler frequency f_d of 10 Hz for simulations and analysis of the performance of the proposed NOMA-SM scheme in V2V communication. The analysis highlights the robustness of the NOMA-SM scheme under various channel conditions. Additionally, a time difference of 0.1 seconds, combined with a Doppler shift of 10 Hz, introduces challenges in channel estimation, increases BER, and causes inefficiencies in power allocation, all of which are critical factors in V2V communication system performance.

2) MIMO System based on NOMA

The study [44] analyzed the performance of various MIMO configurations in NOMA systems at different velocities to enhance system performance, particularly as the number of connected vehicles increases and diverse user velocities need to be supported. The Doppler shift in a V2V communication scenario, as described by (64), is directly influenced by the relative velocity between the transmitter and the receiver.

$$f_d = \pm \frac{f_c V}{C} \cos\theta \tag{64}$$

where, f_d represents the frequency shift observed at the receiver, f_c is the carrier frequency, V denotes the relative velocity between the transmitter and receiver, C is the speed of light (approximately 3×10^8 m/s), and θ is the angle of the velocity vector. Furthermore, the Doppler shift was proportional to the carrier frequency, indicating that higher frequencies experience more significant shifts.

3) OFDM-MIMO System supported by LDPC Channel Code

In [16], a Doppler shift of 300 Hz was introduced to simulate realistic conditions in vehicular environments with moving vehicles. The results highlight the error correction capabilities of LDPC codes for mitigating Doppler-induced errors, which are prevalent in high-speed scenarios.

E. THE PROPOSED NOMA-MIMO SYSTEM SUPPORTED BY QC-LDPC WITHOUT $GIRTH_4$ CHANNEL CODE

In the proposed vehicular communication system, the effect of the Doppler shift is considered, particularly at a frequency of 0.2 THz and a speed of 120 km/h. This results in a frequency change of approximately 22.22 Hz, which can substantially impact the performance of the NOMA-MIMO system. As shown in Fig.11, the Doppler shift effect on a NOMA-MIMO system can be mitigated for high-speed users by applying QC-LDPC codes. By incorporating a longer girth, the structure of the QC-LDPC codes disrupts the belief propagation algorithm used in LDPC decoding, providing efficient decoding that is essential for effective communication in high-speed vehicular environments. These codes, optimized for time-varying channels affected by Doppler shifts, can significantly improve throughput and reduce BER in such dynamic settings.

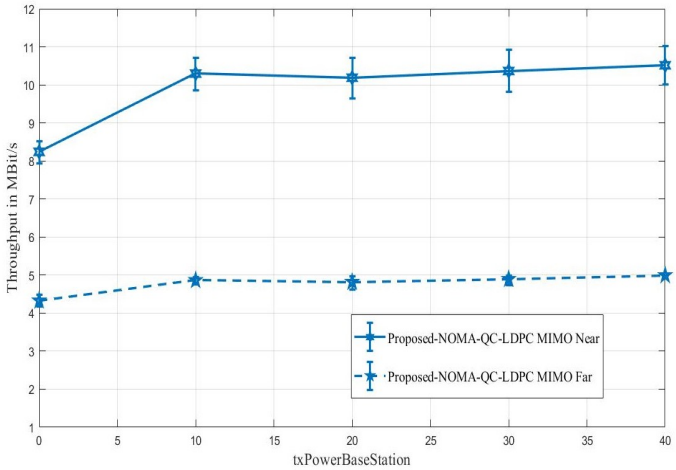

FIGURE 11: Throughput for (Bob_1) (Bob_2) when velocity 120 km/h

XIV. CONCLUSIONS

The proposed system demonstrates superior BER performance in vehicular communication by leveraging the algebraic structure of QC-LDPC codes without $Girth_4$ cycles and the enhanced capabilities of NOMA. The mentioned codes effectively address the challenges of fluctuating channel conditions and high mobility, ensuring reliable and efficient communication. Furthermore, even without clustering, the system maintains low BER and supports high data rates. The study also analyzes the average PEP for both ML and SIC detection techniques, revealing closed-form expressions for both users' sum rates and outage probabilities based on the extracted vectors from the Rician fading MIMO channels. It was observed that the mentioned channel codes achieve superior performance compared to benchmark schemes, particularly at a 1/3 code rate. They approach the Shannon limit, enabling higher data rates without a corresponding increase in errors, which is crucial for maintaining consistent V2V communication under varying vehicle motions. Moreover, codes are designed to be decoded using iterative algorithms with low computational complexity, making them well-suited for V2V communications where processing resources are limited, and low-latency is crucial for applications such as safety messaging and real-time data exchange, which demand high reliability and efficiency.

REFERENCES

[1] P. C. Bao, D. V. X. Huong, D. N. M. Dang, Q. Le Trung, and L. D. Khai, "High throughput and low complexity implementation for uplink scheme of 5g technology," in 2019 26th International Conference on Telecommunications (ICT), pp. 304–308, IEEE, 2019.

[2] U. K. Dey, R. Akl, and R. Chataut, "Performance improvement in cellular v2x (cv2x) by using low density parity check (ldpc) code," in 2022 IEEE 13th Annual Ubiquitous Computing, Electronics & Mobile Communication Conference (UEMCON), pp. 0296–0302, IEEE, 2022.

[3] Y. Saito, A. Benjebbour, Y. Kishiyama, and T. Nakamura, "System-level performance of downlink non-orthogonal multiple access noma under various environments," in 2015 IEEE 81st vehicular technology conference (VTC Spring), pp. 1–5, IEEE, 2015.

[4] F. Kara and H. Kaya, "Spatial multiple access (sma): Enhancing performances of mimo-noma systems," in 2019 42nd International Conference on Telecommunications and Signal Processing (TSP), pp. 466–471, 2019.

[5] Y. Ai, M. Cheffena, A. Mathur, and H. Lei, "On physical layer security of double rayleigh fading channels for vehicular communications," IEEE Wireless Communications Letters, vol. 7, no. 6, pp. 1038–1041, 2018.

[6] K. Semiha and S. Ö. Ata, "Noma-enabled cooperative v2v communications with fixed-gain af relaying," Balkan Journal of Electrical and Computer Engineering, vol. 11, no. 1, pp. 1–12, 2023.

[7] B. E. Y. Belmekki, A. Hamza, and B. Escrig, "Performance analysis of cooperative noma at intersections for vehicular communications in the presence of interference," Ad Hoc Networks, vol. 98, p. 102036, 2020.

[8] Y. A. B. J. Y. Chen, L. Wang and L. Hanzo, "Performance analysis of noma-sm in vehicle-to-vehicle massive mimo channels," Journal on Selected Areas in Communications, vol. 35, no. 12, pp. 2653–2666, 2017.

[9] B. W. Khoueiry and M. R. Soleymani, "An efficient noma v2x communication scheme in the internet of vehicles," in 2017 IEEE 85th Vehicular Technology Conference (VTC Spring), pp. 1–7, IEEE, 2017.

[10] B. E. Y. Belmekki, A. Hamza, and B. Escrig, "On the outage probability of cooperative 5g noma at intersections," in 2019 IEEE 89th Vehicular Technology Conference (VTC2019-Spring), pp. 1–6, IEEE, 2019.

[11] S. Moon, S. Bae, and I. Hwang, "Vehicle mimo system for high reliability and low latency in nr-based ev2x," ISSN: 2308-4219, pp. 32–36, 2018.

[12] R. Gallager, "Low-density parity-check codes," IRE Transactions on information theory, vol. 8, no. 1, pp. 21–28, 1962.

[13] D. J. MacKay and R. M. Neal, "Near shannon limit performance of low density parity check codes," Electronics letters, vol. 33, no. 6, pp. 457–458, 1997.

[14] M. Kizawa and T. Ikegami, "Iterative cancellation for inter-block-interference on ldpc coded mimo-ofdm systems," in 2020 IEEE 91st Vehicular Technology Conference (VTC2020-Spring), pp. 1–5, IEEE, 2020.

[15] S. A. Ghauri, M. E. U. Haq, M. Iqbal, and J. U. Rehman, "Performance analysis of ldpc codes on different channels," in 2014 Eighth International Conference on Next Generation Mobile Apps, Services and Technologies, pp. 235–240, IEEE, 2014.

[16] U. K. Dey, R. Akl, and R. Chataut, "Throughput improvement in vehicular communication by using low density parity check (ldpc) code," in 2022 IEEE 12th Annual Computing and Communication Workshop and Conference (CCWC), pp. 0836–0843, IEEE, 2022.

[17] D. Chatzoulis, C. Chaikalis, D. Kosmanos, K. E. Anagnostou, and G. T. Karetsos, "5g v2x performance comparison for different channel coding schemes and propagation models," Sensors, vol. 23, no. 5, p. 2436, 2023.

[18] N. Khosroshahi and T. A. Gulliver, "Quasi-cyclic low density parity check (ldpc) codes for dedicated short range communication (dsrc) systems," in CCECE 2010, pp. 1–5, IEEE, 2010.

[19] C. I. Chikezie, M. David, and A. U. Usman, "Power allocation optimization in noma system for user fairness in 5g networks," in 2022 IEEE Nigeria 4th International Conference on Disruptive Technologies for Sustainable Development (NIGERCON), pp. 1–4, IEEE, 2022.

[20] C. D. Meyer, Matrix analysis and applied linear algebra. SIAM, 2023.

[21] X. Cheng, Z. Huang, and S. Chen, "Vehicular communication channel measurement, modelling, and application for beyond 5g and 6g," IET Communications, vol. 14, no. 19, pp. 3303–3311, 2020.

[22] M. Koca and H. Sari, "Performance analysis of spatial modulation over correlated fading channels," in 2012 IEEE Vehicular Technology Conference (VTC Fall), pp. 1–5, IEEE, 2012.

[23] Z. Rezki and M.-S. Alouini, "On the capacity of rician fading channels with full channel state information at low snr," in 2012 IEEE International Conference on Communications (ICC), pp. 5706–5710, IEEE, 2012.

[24] M. M. Jabbari and H. Nooralizadeh, "Advantages of mimo channel estimation in rician flat fading environments," in 2011 International Conference on Electronic Devices, Systems and Applications (ICEDSA), pp. 11–16, IEEE, 2011.

[25] P. Yang, Y. Xiao, Y. L. Guan, M. Di Renzo, S. Li, and L. Hanzo, "Multidomain index modulation for vehicular and railway communications: A survey of novel techniques," IEEE Vehicular Technology Magazine, vol. 13, no. 3, pp. 124–134, 2018.

[26] Pushpalatha, Prathyusha, Sindhu, M. J. Khan, I. Singh, and S. Tayal, "Ber performance using bpsk modulation over rayleigh and rician fading channel," in 2022 IEEE 11th International Conference on Communication Systems and Network Technologies (CSNT), pp. 434–437, 2022.

[27] H. Li, B. Bai, X. Mu, J. Zhang, and H. Xu, "Algebra-assisted construction of quasi-cyclic ldpc codes for 5g new radio," IEEE Access, vol. 6, pp. 50229–50244, 2018.

[28] Y. Xiao and M. H. Lee, "Construction of good quasi-cyclic ldpc codes," in 2006 IET International Conference on Wireless, Mobile and Multimedia Networks, pp. 1–4, 2006.

[29] S. J. Johnson and S. R. Weller, "Quasi-cyclic ldpc codes from difference families," 2002.

[30] J. Fan, Y. Xiao, and K. Kim, "Design ldpc codes without cycles of length 4 and 6," J. Electr. Comput. Eng., vol. 2008, 2008.

[31] D. J. MacKay, Information theory, inference and learning algorithms. Cambridge university press, 2003.

[32] C. Zhang, L. Ge, X. Zhang, W. Wei, J. Zhao, Z. Zhang, Z. Wang, and X. You, "A uniform molecular low-density parity check decoder," ACS Synthetic Biology, vol. 8, no. 1, pp. 82–90, 2018.

[33] T. L. Narasimhan, P. Raviteja, and A. Chockalingam, "Generalized spatial modulation in large-scale multiuser mimo systems," IEEE Transactions on Wireless Communications, vol. 14, no. 7, pp. 3764–3779, 2015.

[34] A. Almohamad, M. O. Hasna, S. Althunibat, and K. Qaraqe, "A novel downlink im-noma scheme," IEEE Open Journal of the Communications Society, vol. 2, pp. 235–244, 2021.

[35] S. Althunibat, R. Mesleh, and T. F. Rahman, "A novel uplink multiple access technique based on index-modulation concept," IEEE Transactions on Communications, vol. 67, no. 7, pp. 4848–4855, 2019.

[36] A. Almohamad, S. Althunibat, M. Hasna, and K. Qaraqe, "A downlink index-modulation based nonorthogonal multiple access scheme," in 2020 IEEE 31st Annual International Symposium on Personal, Indoor and Mobile Radio Communications, pp. 1–6, IEEE, 2020.

[37] D. Zhang, Z. Zhou, C. Xu, Y. Zhang, J. Rodriguez, and T. Sato, "Capacity analysis of noma with mmwave massive mimo systems," IEEE Journal on Selected Areas in Communications, vol. 35, no. 7, pp. 1606–1618, 2017.

[38] M. H. Kumar, S. Sharma, and M. Thottappan, "Downlink index modulation aided noma for mimo transmission," in 2020 IEEE 3rd 5G World Forum (5GWF), pp. 530–535, IEEE, 2020.

[39] V. Thangasamy, I. Singh, J. Sai, et al., "Analysis of capacity and outage probability for noma based cellular communication over rician fading channel," in 2022 First International Conference on Electrical, Electronics, Information and Communication Technologies (ICEEICT), pp. 1–5, IEEE, 2022.

[40] N. K. Breesam, W. A. Al-Hussaibi, F. H. Ali, and I. M. Al-Musawi, "Efficient resource allocation for wireless-powered mimo-noma communications," IEEE Access, vol. 10, pp. 130302–130313, 2022.

[41] K. Srinivasarao and M. Surendar, "Outage analysis of downlink non-orthogonal multiple access scheme over rician fading channel," in 2020 IEEE 4th Conference on Information Communication Technology (CICT), pp. 1–5, 2020.

[42] B. Kumbhani and R. Kshetrimayum, MIMO Wireless Communications Over Generalized Fading Channels. CRC Press, Taylor & Francis Group, 2017.

[43] M. D. Yacoub, "The κ-μ distribution and the η-μ distribution," IEEE Antennas and Propagation Magazine, vol. 49, pp. 68–81, 2007.

[44] R. A. Hussein and S. A. Ayoob, "Doppler shift effect with non-orthogonal multiple access technology for 5g system," in Proceedings of the 2nd International Multi-Disciplinary Conference Theme: Integrated Sciences and Technologies, IMDC-IST 2021, 7-9 September 2021, Sakarya, Turkey, IMDC-IST, EAI, Jan. 2022.

MARYAM MOHAMMED F. ABDULLAH received her B.Sc. degree in the Information Engineering Department at Al-Khwarizmi College of Engineering, University of Baghdad, Iraq, in 2004–2005, and her M.Sc. degree in Laser Applications/Electronics and Communications from the Institute of Laser for Postgraduate Studies, University of Baghdad, Iraq, in 2007. Her research focused on implementing quantum cryptographic (QC) systems based on the BB84 protocol. She was a lecturer in the Electrical Engineering Department at Kirkuk University, Kirkuk, Iraq. She is currently pursuing a Ph.D. degree in the Department of Electrical and Electronics Engineering, Ankara University, Ankara, Turkey. Her current research interests include the performance analysis of vehicular communications based on NOMA-MIMO techniques and the effectiveness of QC-LDPC channel coding in vehicular communication environments.

OSAMA ALLUHAIBI received the B.E. degree in electrical and communications engineering from the University of Baghdad, Iraq, in 2006, the M.Sc. degree in electronics and communications engineering from the Sam Higginbottom Institute of Agriculture, Technology and Sciences, India, in 2012, and the Ph.D. degree in electronics and communications engineering from the University of Kent, Canterbury, U.K., in 2018. From 2007 to 2010, he was associated with ABB Group, and Kalimat Telecom. In July 2018, he joined the Connectivity Group, WMG's Intelligent Vehicles Research Team, University of Warwick, U.K., as a Research Fellow. His research interests include hybrid beamforming, performance analysis of 5G millimeter-wave wireless communications systems, and 5G millimeter-wave communication for the Industrial Internet of Things applications.

ASIM EGEMEN YILMAZ is affiliated with the Department of Electrical and Electronics Engineering at Ankara University. He has received his B.Sc., M.Sc., and Ph.D. degrees in electrical–electronics engineering and mathematics from Middle East Technical University. His areas of expertise include computational electromagnetics and optimization.

AYKUT KALAYCIOGLU received a B.Sc. degree from Ankara University, Ankara, Turkey, an M.Sc. degree from the University of Pittsburgh, PA, USA, and a Ph.D. degree from Ankara University, Ankara, Turkey. He is an assistant professor at the Electrical Electronics Engineering Department, at Ankara University. His research interests include wireless communication systems and cellular networks.